

A Statistical Benchmark for Diffusion Posterior Sampling Algorithms

Martin Zach, Youssef Haouchat, Michael Unser

Abstract—We propose a statistical benchmark for diffusion posterior sampling (DPS) algorithms for Bayesian linear inverse problems. The benchmark synthesizes signals from sparse Lévy-process priors whose posteriors admit efficient Gibbs methods. These Gibbs methods can be used to obtain gold-standard posterior samples that can be compared to the samples obtained by the DPS algorithms. By using the Gibbs methods for the resolution of the denoising problems in the reverse diffusion, the framework also isolates the error that arises from the approximations to the likelihood score. We instantiate the benchmark with the minimum-mean-squared-error optimality gap and posterior coverage tests and provide numerical experiments for popular DPS algorithms on the inverse problems of denoising, deconvolution, imputation, and reconstruction from partial Fourier measurements. We release the benchmark code at <https://github.com/zacmar/dps-benchmark>. The repository exposes simple plug-in interfaces, reference scripts, and config-driven runs so that new algorithms can be added and evaluated with minimal effort. We invite researchers to contribute and report results.

Index Terms—Diffusion models, Bayesian inverse problems, statistical evaluation, Gibbs sampling.

I. INTRODUCTION

DIFFUSION models are among the leading generative models in imaging [1], visual computing [2], finance and time-series analysis [3], [4], de novo protein and drug design [5], [6], natural language processing [7], [8], and other domains. Their ability to model complex distributions has motivated their use as priors in Bayesian inverse problems in those domains. In fact, reconstruction methods that leverage diffusion models are competitive or state-of-the-art in, *e.g.*, deconvolution [9], phase retrieval [10], magnetic resonance imaging and computed tomography reconstruction [11], [12], weather-artifact removal [13], task-conditioned protein design [14], audio bandwidth extension and dereverberation [15], and denoising of financial time-series [16].

Despite this empirical success, diffusion models lack a natural strategy of conditioning on the measurements and active research explores how to incorporate the likelihood [17], [18]. Currently, conditioning strategies are evaluated in one of two ways. (i) With respect to downstream applications: As an example, evaluations with respect to perceptual metrics such as the structural similarity [19], the Fréchet inception distance [20], or the learned perceptual image patch similarity [21] are common in the imaging sciences. However, as pointed out in [22], they are ill-suited for the statistical evaluation of the ability of algorithms to sample from the posterior distribution. Such a statistical evaluation is critical in high-stakes applications such

as medical imaging or remote sensing, where decisions based on reconstructions and their associated uncertainties may have significant consequences. (ii) In overly simplistic settings: A common fallback is to evaluate in synthetic settings with finite Gaussian mixture priors (often with only one component, like in the theoretical analysis in [22], or many components, like in the empirical evaluation in, *e.g.*, [23, Section E.3] or [24]). Such finite Gaussian mixtures remain light-tailed with the tail decreasing exponentially like the widest component and, consequently, they cannot reproduce power-law-like extremes that are common in, *e.g.*, asset returns [25], [26] or the statistics of images [27]. Benchmarks built on such priors can therefore overstate posterior quality.

We propose a statistical evaluation framework for DPS algorithms for Bayesian linear inverse problems that addresses these issues. We synthesize signals from discretized sparse Lévy-process priors for which the resulting posteriors can be sampled from efficiently. Indeed, they admit efficient Gibbs methods with exact conditionals that provide gold-standard posterior samples. The framework supports general posterior-level comparisons—*e.g.*, (sliced) Wasserstein or energy distances or calibration via coverage or posterior predictive checks—by furnishing matched samples obtained from the DPS algorithms and the gold-standard Gibbs methods. In this paper, we instantiate the framework with two simple metrics: the minimum-mean-squared error (MMSE) optimality gap and highest posterior density coverage checks across the inverse problems of denoising, deconvolution, imputation, and reconstruction from partial Fourier measurements. Moreover, the framework enables the isolation of the error that is attributable to the likelihood-score approximation by replacing the learned denoiser with an oracle MMSE denoiser computed from Gibbs samples at each reverse-diffusion step.

A. Contributions

We build on the statistical framework introduced in [28] that benchmarked various neural network-based and model-based MMSE point estimators and provided optimality gaps by leveraging gold-standard estimators obtained by the Gibbs methods. We generalize this benchmark from MMSE point estimators to posterior samplers and thereby enable the comparison of different methods on the distribution level instead of the point-estimation level.

To disentangle error sources within DPS algorithms, we replace any learned denoiser with an oracle MMSE denoiser that is computed via the Gibbs methods at each reverse-diffusion step. This isolates the error due to the likelihood-score approximation from the error due to the prior-score surrogate.

To accommodate those DPS algorithms within our framework that do not follow a strict split between prior and likelihood—such as diffusion plug-and-play (DPnP) [29]—we introduce a

M. Zach, Y. Haouchat, and M. Unser are with the Biomedical Imaging Group, École Polytechnique Fédérale de Lausanne, 1015 Lausanne, Switzerland. (e-mail: martin.zach@epfl.ch; youssef.haouchat@epfl.ch; michael.unser@epfl.ch)

M. Zach is with the Center for Biomedical Imaging, 1015 Lausanne, Switzerland.

new template for DPS algorithms that utilize *samples* from the denoising problem in their update steps, as opposed to only the MMSE point estimate. This template arises naturally in our framework because Gibbs methods already provide these denoising-posterior samples and we show how several popular DPS algorithms can be re-expressed within this template.

Finally, we instantiate the benchmark with the MMSE optimality gap and posterior coverage tests. We report results on denoising, deconvolution, imputation, and reconstruction from partial Fourier measurements, with and without learned components and provide an online repository that contains the open-source benchmarking code that is deliberately designed to facilitate the benchmarking of novel algorithms.

II. BACKGROUND

A. Bayesian Linear Inverse Problems

We seek to estimate a signal $\mathbf{x} \in \mathbb{R}^d$ from the measurements

$$\mathbf{y} = \mathbf{A}\mathbf{x} + \mathbf{n}, \quad (1)$$

where the *forward operator* $\mathbf{A} \in \mathbb{R}^{m \times d}$ models the noiseless linear measurement acquisition and $\mathbf{n} \in \mathbb{R}^m$ is additive noise. In the Bayesian treatment of this problem, the signals are modeled as a random variable, denoted \mathbf{X} , with values in \mathbb{R}^d and distribution $p_{\mathbf{X}}$. We refer to $p_{\mathbf{X}}$ as the *prior*. Given any datum \mathbf{y} , the ultimate goal is to analyze the *posterior* $p_{\mathbf{X}|\mathbf{Y}=\mathbf{y}}$ which is related to the *likelihood* $p_{\mathbf{Y}|\mathbf{X}=\mathbf{x}}$ and the prior $p_{\mathbf{X}}$ via Bayes' rule, which states that

$$p_{\mathbf{X}|\mathbf{Y}=\mathbf{y}}(\mathbf{x}) \propto p_{\mathbf{Y}|\mathbf{X}=\mathbf{x}}(\mathbf{y})p_{\mathbf{X}}(\mathbf{x}). \quad (2)$$

For a given signal \mathbf{x} , the likelihood $p_{\mathbf{Y}|\mathbf{X}=\mathbf{x}}$ is determined by the distribution of the noise. A common assumption on the noise is that it is a vector of independent and identically distributed (i.i.d.) Gaussian random variables with mean zero and variance $\sigma_{\mathbf{n}}^2$.¹ In this case, the likelihood is given by

$$p_{\mathbf{Y}|\mathbf{X}=\mathbf{x}}(\mathbf{y}) \propto \exp\left(-\frac{1}{2\sigma_{\mathbf{n}}^2}\|\mathbf{A}\mathbf{x} - \mathbf{y}\|^2\right). \quad (3)$$

Thus, once the forward model and the noise law are specified, the remaining modeling choice is the prior distribution. The ability of diffusion models to model complex distributions makes them a good candidate prior for the resolution of inverse problems. However the lack of a natural conditioning mechanism prohibits a straightforward use, see [section II-D](#).

B. Bayes Estimators

A benefit of the Bayesian approach over classical variational methods (see, e.g., [30]) is that different point estimates arise from a fixed prior. For a given measurement \mathbf{y} , these point estimates summarize the posterior distribution $p_{\mathbf{X}|\mathbf{Y}=\mathbf{y}}$ with respect to a given loss $\ell : \mathbb{R}^d \times \mathbb{R}^d \rightarrow \mathbb{R}$ via the optimization problem of finding the point $\hat{\mathbf{x}}_{\ell}(\mathbf{y})$ that minimizes the posterior risk:

$$\hat{\mathbf{x}}_{\ell}(\mathbf{y}) = \arg \min_{\hat{\mathbf{x}} \in \mathbb{R}^d} \left(\int_{\mathbb{R}^d} \ell(\hat{\mathbf{x}}, \mathbf{x}) p_{\mathbf{X}|\mathbf{Y}=\mathbf{y}}(\mathbf{x}) d\mathbf{x} \right). \quad (4)$$

¹Our framework supports more general (possibly non-Gaussian) likelihoods, see [section IV-A](#).

In this paper, the Bayes estimator with respect to the mean-squared error (MSE) $\ell = \frac{1}{d}\|\cdot - \cdot\|^2$ plays a key role due to its close relation to the prior *score* in the reverse diffusion (see [section II-C](#)) and because we later quantify the performance of DPS algorithms via an MMSE optimality gap. With this choice of ℓ , (4) can be written as

$$\begin{aligned} \hat{\mathbf{x}}_{\text{MMSE}}(\mathbf{y}) &= \arg \min_{\hat{\mathbf{x}} \in \mathbb{R}^d} \left(\int_{\mathbb{R}^d} \frac{1}{d}\|\hat{\mathbf{x}} - \mathbf{x}\|^2 p_{\mathbf{X}|\mathbf{Y}=\mathbf{y}}(\mathbf{x}) d\mathbf{x} \right) \\ &= \int_{\mathbb{R}^d} \mathbf{x} p_{\mathbf{X}|\mathbf{Y}=\mathbf{y}}(\mathbf{x}) d\mathbf{x} = \mathbb{E}[\mathbf{X} | \mathbf{Y} = \mathbf{y}], \end{aligned} \quad (5)$$

which is the expectation of the posterior $p_{\mathbf{X}|\mathbf{Y}=\mathbf{y}}$.

Another widely-used estimator arises through the choice

$$\ell(\hat{\mathbf{x}}, \mathbf{x}) = -\chi_{\{\hat{\mathbf{x}}\}}(\mathbf{x}) \quad (6)$$

where

$$\chi_A(\mathbf{x}) := \begin{cases} 1 & \text{if } \mathbf{x} \in A, \\ 0 & \text{else,} \end{cases} \quad (7)$$

which leads to the maximum-a-posteriori (MAP) estimator that seeks the mode of the posterior:²

$$\begin{aligned} \hat{\mathbf{x}}_{\text{MAP}}(\mathbf{y}) &= \arg \min_{\hat{\mathbf{x}} \in \mathbb{R}^d} \left(\int_{\mathbb{R}^d} -\chi_{\{\hat{\mathbf{x}}\}}(\mathbf{x}) p_{\mathbf{X}|\mathbf{Y}=\mathbf{y}}(\mathbf{x}) d\mathbf{x} \right) \\ &= \arg \max_{\mathbf{x} \in \mathbb{R}^d} p_{\mathbf{X}|\mathbf{Y}=\mathbf{y}}(\mathbf{x}). \end{aligned} \quad (8)$$

Rewriting (8) as

$$\hat{\mathbf{x}}_{\text{MAP}} = \arg \min_{\mathbf{x} \in \mathbb{R}^d} \left(-\frac{1}{2\sigma_{\mathbf{n}}^2}\|\mathbf{A}\mathbf{x} - \mathbf{y}\|^2 - \log p_{\mathbf{X}}(\mathbf{x}) \right), \quad (9)$$

reveals a close relation to classical variational approaches after identifying the regularizer with $-\log p_{\mathbf{X}}$.

C. Diffusion Models

As the likelihood is modeled explicitly in Bayesian inverse problems, the modeling burden lies with the prior. Diffusion models are widely used to synthesize new signals that usefully generalize the training distribution and have proven effective across domains, which motivates their use as priors. We first give a background on diffusion models and then describe the problem that arises when using these models in Bayesian inverse problems in [section II-D](#).

Diffusion models were introduced by Song et al. in [33] by unifying the discrete approaches presented in [34] and [35] in a continuous theory based on stochastic differential equations (SDEs). In the sequel, we only introduce those concepts of SDEs that are relevant for the present work and refer to [36, Chapters 25 and 26] for more details. We denote the (diffusion) SDE with *drift coefficient* $\mathbf{f} : \mathbb{R}^d \times \mathbb{R}_{\geq 0} \rightarrow \mathbb{R}^d$ and *diffusion coefficient* $g : \mathbb{R}_{\geq 0} \rightarrow \mathbb{R}$ as

$$d\mathbf{X}_t = \mathbf{f}(\mathbf{X}_t, t) dt + g(t) d\mathbf{W}_t, \quad (10)$$

²This definition is informal but sufficient for the purposes of this paper. For continuous posteriors, the strict 0–1 loss Bayes' rule is ill-posed. A common formalization defines MAP as the limit of Bayes estimators under shrinking small-ball 0–1 losses; under additional regularity, this limit agrees with the posterior mode [31], [32]. The MAP estimator may also not be unique.

where \mathbf{W}_t is the standard Wiener process. A solution to that SDE is a stochastic process $(\mathbf{X}_t)_t$ that satisfies the integral equation

$$\mathbf{X}_t = \mathbf{X}_0 + \int_0^t \mathbf{f}(\mathbf{X}_s, s) ds + \int_0^t g(s) d\mathbf{W}_s \quad (11)$$

for some suitable initial condition \mathbf{X}_0 . In our setup, the initial condition is the random variable that describes the signal, thus $\mathbf{X}_0 = \mathbf{X}$. Under suitable choices for \mathbf{f} and g , the forward process admits a limiting marginal \mathbf{X}_∞ as $t \rightarrow \infty$. Sampling from $p_{\mathbf{X}_0}$ can then proceed by simulating the SDE (10) in reverse with initial condition \mathbf{X}_∞ . By Anderson's theorem [37], the reverse SDE that reproduces the forward marginals satisfies

$$d\mathbf{X}_t = (\mathbf{f}(\mathbf{X}_t, t) - g^2(t) \nabla \log p_{\mathbf{X}_t}(\mathbf{X}_t)) dt + g(t) d\mathbf{W}_t, \quad (12)$$

where $p_{\mathbf{X}_t}$ denotes the density of \mathbf{X}_t from (11), and dt is an infinitesimal negative time step.

The primary challenge in this approach lies in the computation of the *scores* $\nabla \log p_{\mathbf{X}_t}$ for all $t > 0$. We now derive an equality that relates $\nabla \log p_{\mathbf{X}_t}$ to $\mathbb{E}[\mathbf{X}_0 | \mathbf{X}_t = \cdot]$, i.e., the MMSE estimate of \mathbf{X}_0 given that \mathbf{X}_t takes on a certain value. We restrict ourselves to the drift coefficient $\mathbf{f}(\mathbf{x}, t) = -\frac{\beta(t)}{2} \mathbf{x}$ and the diffusion coefficient $g(t) = \sqrt{\beta(t)}$, which correspond to the *variance-preserving* formulation (see [33, Section 3.4]) whose limiting marginal is the standard normal (which is preferred for its numerical properties) and where $\beta : \mathbb{R}_{\geq 0} \rightarrow \mathbb{R}_{\geq 0}$ controls how fast the process contracts towards zero and how much noise is injected. Similar derivations can be found in, e.g., [33], [38], [39], but we include it to underscore the relevance of the MMSE estimate in this paper and to facilitate the understanding of its relation to various objects. Under this choice of the drift and diffusion coefficient, the diffusion SDE (10) simplifies to a time-inhomogeneous Ornstein–Uhlenbeck SDE (see [36, Example 26.5])

$$d\mathbf{X}_t = -\frac{\beta(t)}{2} \mathbf{X}_t dt + \sqrt{\beta(t)} d\mathbf{W}_t, \quad (13)$$

whose pathwise solution

$$\mathbf{X}_t = \alpha(t) \mathbf{X}_0 + \int_0^t \frac{\alpha(t)}{\alpha(s)} \sqrt{\beta(t)} d\mathbf{W}_s \quad (14)$$

where $\alpha(t) = \exp(-\frac{1}{2} \int_0^t \beta(s) ds)$ can be computed with standard techniques, see, e.g., [40, Section 4.4.4]. In addition, since

$$\begin{aligned} & \int_0^t \left(\frac{\alpha(t)}{\alpha(s)} \right)^2 \beta(t) ds \\ &= \int_0^t \beta(s) \exp\left(-\int_s^t \beta(u) du\right) ds = 1 - \alpha^2(t) \end{aligned} \quad (15)$$

we can write that

$$\mathbf{X}_t = \alpha(t) \mathbf{X}_0 + \sigma(t) \mathbf{N} \quad (16)$$

in distribution, where $\sigma^2(t) = 1 - \alpha^2(t)$. Consequently, the density of \mathbf{X}_t is given by the convolution of $p_{\mathbf{X}_0}$ with a Gaussian with variance $\sigma^2(t)$ and appropriate scaling by $\alpha(t)$:

$$p_{\mathbf{X}_t}(\mathbf{x}) = \int_{\mathbb{R}^d} g_{0, \sigma(t)^2}(\mathbf{x} - \alpha(t) \hat{\mathbf{x}}) p_{\mathbf{X}_0}(\hat{\mathbf{x}}) d\hat{\mathbf{x}}, \quad (17)$$

where $g_{\boldsymbol{\mu}, \boldsymbol{\Sigma}}(\mathbf{x}) = (2\pi)^{-\frac{d}{2}} |\boldsymbol{\Sigma}|^{-\frac{1}{2}} \exp(-\frac{1}{2} \|\mathbf{x} - \boldsymbol{\mu}\|_{\boldsymbol{\Sigma}^{-1}}^2)$. Finally, after taking the gradient we see that

$$\begin{aligned} \nabla p_{\mathbf{X}_t}(\mathbf{x}) &= \int_{\mathbb{R}^d} \nabla g_{0, \sigma(t)^2}(\mathbf{x} - \alpha(t) \hat{\mathbf{x}}) p_{\mathbf{X}_0}(\hat{\mathbf{x}}) d\hat{\mathbf{x}} \\ &= \int_{\mathbb{R}^d} \left(-\frac{1}{\sigma^2(t)} (\mathbf{x} - \alpha(t) \hat{\mathbf{x}}) g_{0, \sigma^2(t)}(\mathbf{x} - \alpha(t) \hat{\mathbf{x}}) p_{\mathbf{X}_0}(\hat{\mathbf{x}}) d\hat{\mathbf{x}} \right. \\ &= -\frac{1}{\sigma^2(t)} \left(\mathbf{x} p_{\mathbf{X}_t}(\mathbf{x}) - \right. \\ &\quad \left. \alpha(t) \int_{\mathbb{R}^d} \hat{\mathbf{x}} g_{0, \sigma^2(t)}(\mathbf{x} - \alpha(t) \hat{\mathbf{x}}) p_{\mathbf{X}_0}(\hat{\mathbf{x}}) d\hat{\mathbf{x}} \right) \\ &= -\frac{1}{\sigma(t)^2} \left(\mathbf{x} p_{\mathbf{X}_t}(\mathbf{x}) - \alpha(t) p_{\mathbf{X}_t}(\mathbf{x}) \mathbb{E}[\mathbf{X}_0 | \mathbf{X}_t = \mathbf{x}] \right) \end{aligned} \quad (18)$$

such that, after dividing by $p_{\mathbf{X}_t}(\mathbf{x})$ and since $\frac{\nabla p_{\mathbf{X}_t}(\mathbf{x})}{p_{\mathbf{X}_t}(\mathbf{x})} = \nabla \log p_{\mathbf{X}_t}(\mathbf{x})$, we find the celebrated Tweedie identity

$$\nabla \log p_{\mathbf{X}_t}(\mathbf{x}) = -\sigma(t)^{-2} (\mathbf{x} - \alpha(t) \mathbb{E}[\mathbf{X}_0 | \mathbf{X}_t = \mathbf{x}]). \quad (19)$$

Thus, given any point \mathbf{x} and time $t > 0$, this yields a practical way of computing $\nabla \log p_{\mathbf{X}_t}(\mathbf{x})$ through the resolution of the MMSE denoising problem of finding $\mathbb{E}[\mathbf{X}_0 | \mathbf{X}_t = \mathbf{x}]$.

In standard applications where the goal is the generation of new signals, this MMSE denoising problem is typically tackled through the off-line learning of the map $(\mathbf{x}, t) \mapsto \mathbb{E}[\mathbf{X}_0 | \mathbf{X}_t = \mathbf{x}]$ via a neural network.³ In our benchmark, we instead obtain oracle MMSE denoisers via Gibbs methods and thereby eliminate approximation errors from a learned surrogate when isolating error sources in DPS algorithms.

1) *Discretization*: Implementing the reverse SDE for generation requires a time discretization, which is typically done by Euler–Maruyama techniques (see, e.g., [42]). For the reverse Ornstein–Uhlenbeck SDE

$$d\mathbf{X}_t = \left(-\frac{\beta(t)}{2} \mathbf{X}_t - \beta(t) \nabla \log p_{\mathbf{X}_t}(\mathbf{X}_t) \right) dt + \sqrt{\beta(t)} d\mathbf{W}_t, \quad (20)$$

a first-order step from t to $t - 1$ ($dt = -1$) gives the Euler–Maruyama update

$$\mathbf{X}_{t-1} = \left(1 + \frac{\beta_t}{2} \right) \mathbf{X}_t + \beta_t \nabla \log p_{\mathbf{X}_t}(\mathbf{X}_t) + \sqrt{\beta_t} \mathbf{Z}_t, \quad (21)$$

where $\beta_t := \beta(t)$ and $\mathbf{Z}_t \sim \text{Gauss}(\mathbf{0}, \mathbf{I})$.

In practice, researchers typically use an alternative schedule from the discrete-time Markov chain that was initially proposed by Sohl-Dickstein et al. in [43] and revisited and popularized by Ho et al. in [35]. There, the discretization

$$\mathbf{X}_{t-1} = \frac{1}{\sqrt{1-\beta_t}} (\mathbf{X}_t + \beta_t \nabla \log p_{\mathbf{X}_t}(\mathbf{X}_t)) + \sqrt{\beta_t} \mathbf{Z}_t, \quad (22)$$

is used and typically called denoising diffusion probabilistic model (DDPM)-style sampling. It can be related to the Euler–Maruyama discretization of the SDE via Taylor expansions; we provide a detailed derivation in [appendix A](#).

We show a trajectory of signals generated by this discretization of the reverse SDE using the oracle MMSE denoiser in [fig. 1](#). The signals and the construction of the MMSE

³This does not necessitate the off-line computation of any MMSE denoising result since it can be implemented by finding that f that minimizes $\int_{t>0} \mathbb{E}_{(\mathbf{X}_t, \mathbf{X}_0)} [\|f(\mathbf{X}_t, t) - \mathbf{X}_0\|^2]$, where a pair $(\mathbf{X}_t, \mathbf{X}_0)$ from the joint distribution can be constructed through ancestral sampling (i.e., sampling \mathbf{X}_0 and setting \mathbf{X}_t according to (16)) [41].

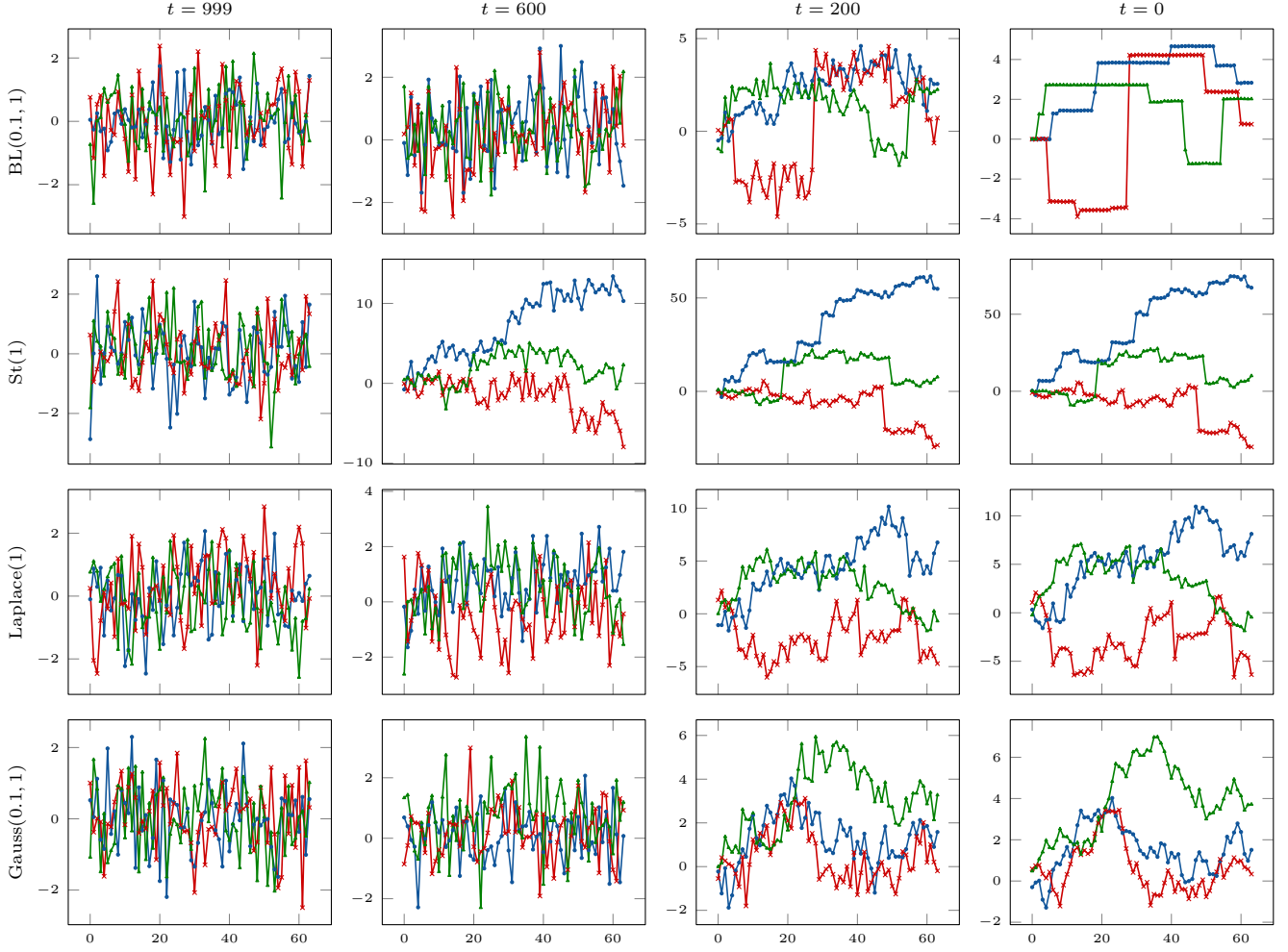


Fig. 1: Unconditional reverse-diffusion trajectories obtained by DDPM sampling with the oracle denoiser. Rows: Jump distributions. Columns: Diffusion times. Line styles: Different initializations and random states.

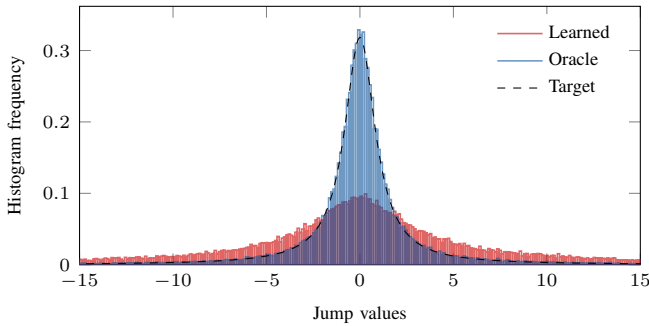


Fig. 2: Histogram of jumps of signals obtained by unconditional DDPM sampling with the oracle denoiser and the learned denoiser.

denoiser are described in [section IV](#). To motivate our use of the oracle MMSE denoiser, we show in [fig. 2](#) a histogram of jump distributions obtained by the learned denoiser versus the oracle denoiser for a $St(1)$ jump target (our notations of various distributions is summarized in [table V](#)). The signals generated by the oracle denoiser follow the jump distribution almost perfectly since the reverse diffusion is an exact sampler

up to discretization error. Example generated signals are shown in [fig. 8](#) in the appendix.

D. Diffusion Posterior Sampling

The reverse-diffusion sampler from the previous section can be adapted to sample from a posterior by replacing the prior score $\nabla \log p_{\mathbf{X}_t}$ with the posterior score $\nabla \log p_{\mathbf{X}_t|\mathbf{Y}=\mathbf{y}}$ for some given measurement \mathbf{y} . An inspection of $\nabla \log p_{\mathbf{X}_t|\mathbf{Y}=\mathbf{y}}$ via Bayes' theorem reveals that

$$\nabla \log p_{\mathbf{X}_t|\mathbf{Y}=\mathbf{y}} = \nabla \log p_{\mathbf{X}_t} + \nabla (\mathbf{x} \mapsto \log p_{\mathbf{Y}|\mathbf{X}_t=\mathbf{x}}(\mathbf{y})). \quad (23)$$

Although the dependence between \mathbf{Y} and \mathbf{X}_0 is known through [\(1\)](#) and the likelihood is explicitly modeled via [\(3\)](#), it is generally challenging to relate \mathbf{Y} and \mathbf{X}_t for any $t > 0$ with an explicit likelihood. Thus, the conditioning on the measurements (or, more generally, on various characteristics of the solution like a desired fitness value in de novo protein design) is usually done in one of two ways:

- 1) A learned component directly models the posterior score and gets the measurements (or a quantity derived thereof) as input. This strategy is pursued in, *e.g.*, [\[12\]](#)–[\[14\]](#), [\[44\]](#),

and is advantageous when the measurement process is unknown, difficult to model, or prohibitively expensive to evaluate. However, reconstructions obtained by this strategy typically degrade under shifts in measurement conditions, since the learned components cannot adapt to the new measurement conditions.

- 2) The Bayesian separation that is described in [section II-A](#) is pursued. This is done in, *e.g.*, [10], [11] and the methods reviewed in [15], and is advantageous when the measurement process is known, relatively inexpensive to evaluate, and subject to change, but prior knowledge should be reused, which is frequently the case in, *e.g.*, imaging or remote sensing applications. However, this requires approximations to $\nabla(\mathbf{x} \mapsto \log p_{\mathbf{Y}|\mathbf{X}_t=\mathbf{x}}(\mathbf{y}))$ for all $t > 0$.

As an example, in [45] Jalal et al. proposed the approximation

$$\nabla(\mathbf{x} \mapsto \log p_{\mathbf{Y}|\mathbf{X}_t=\mathbf{x}}(\mathbf{y})) \approx \nabla(\mathbf{x} \mapsto \log p_{\mathbf{Y}|\mathbf{X}_0=\mathbf{x}}(\mathbf{y})). \quad (24)$$

Another very popular approximation, known under the (unfortunately very generic) name “diffusion posterior sampling” was proposed by Chung et al. in [38]. There, the likelihood is approximated with

$$\begin{aligned} \nabla(\mathbf{x} \mapsto \log p_{\mathbf{Y}|\mathbf{X}_t=\mathbf{x}}(\mathbf{y})) \\ \approx \nabla(\mathbf{x} \mapsto \log p_{\mathbf{Y}|\mathbf{X}_0=\mathbb{E}[\mathbf{X}_0|\mathbf{X}_t=\mathbf{x}]}(\mathbf{y})). \end{aligned} \quad (25)$$

To avoid confusion with the umbrella term of DPS algorithms, we abbreviate that specific method as Chung diffusion posterior sampling (C-DPS). The approximation that is made in diffusion models for plug-and-play image restoration (DiffPIR) [46] is to take the Moreau envelope of the potential of $p_{\mathbf{Y}|\mathbf{X}_0=\cdot}(\mathbf{y})$ and evaluating its gradient at $\mathbb{E}[\mathbf{X}_0 | \mathbf{X}_t = \cdot]$.

In principle, our benchmark can evaluate either strategy (and any other method that claims to sample from a posterior distribution). The first approach, however, relies on black-box learning of the conditional posterior score and its performance heavily depends on various implementation details. Thus, we primarily focus on the second approach that necessitates approximations of the likelihood score (and more general DPS algorithms with some kind of explicit conditioning, see our proposed generalization in [section II-E](#)). Our framework supplies reference objects—posterior samples and oracle denoisers via Gibbs methods—to isolate and quantify the impact of these approximations in DPS algorithms.

E. A Generalization to Accommodate More Algorithms

The description in the previous section—approximating the likelihood score inside the reverse diffusion—covers the family of algorithms named “explicit approximations for measurement matching” in the recent survey [47]. However, widely used methods such as DPnP [29], fall outside this pattern. We therefore introduce a simple template that accommodates a broader set of DPS algorithms and is natural in our setting, where the denoising posterior is *sampled* via Gibbs methods.

We characterize DPS algorithms as an iteration rule that can be summarized into a two-stage process: Given an iterate \mathbf{x}_t with associated noise variance $\sigma^2(t)$, the computation of the next iterate \mathbf{x}_{t-1} is done by

Algorithm 1 Template for DPS algorithms.

Require: Initial point $\mathbf{x}_T, \mathbf{y}, \mathbf{A}, \Theta, \{\sigma_t\}_{t=0}^T$
1: **for** $t = T, \dots, 1$ **do** \triangleright Diffusion process
2: Sample $\{\bar{\mathbf{x}}_k\}_{k=1}^S \sim \exp(-\frac{\|\cdot - \mathbf{x}_t\|^2}{2\sigma_t^2}) p_{\mathbf{X}_0}(\cdot)$
3: Update $\mathbf{x}_{t-1} = \mathcal{S}(\mathbf{x}_t, \{\bar{\mathbf{x}}_k\}_{k=1}^S, \mathbf{y}, \mathbf{A}, \Theta, t)$
4: **return** \mathbf{x}_0 \triangleright Posterior sample

- 1) drawing S samples denoted $\{\bar{\mathbf{x}}_k\}_{k=1}^S$ from the denoising posterior $p_{\mathbf{X}_0|\mathbf{X}_t=\mathbf{x}_t} \propto \exp(-\frac{1}{2\sigma_t^2}\|\cdot - \mathbf{x}_t\|^2) p_{\mathbf{X}_0}(\cdot)$, and
- 2) computing the next iterate \mathbf{x}_{t-1} through an update step \mathcal{S} that may utilize the current iterate \mathbf{x}_t , the samples $\{\bar{\mathbf{x}}_k\}_{k=1}^S$, the measurements \mathbf{y} , the forward operator \mathbf{A} , and any other possible algorithm-internal parameters such as a scalar that weights likelihood and prior terms or parameters that define the noise schedule.

This template is summarized in [algorithm 1](#) and the specialized instances for the step \mathcal{S} that correspond to the three popular algorithms C-DPS [38], DiffPIR [46], and DPnP [29] are tabulated in [table I](#). We have absorbed the scaling by α_t into the step \mathcal{S} since this template is not fundamentally limited to Ornstein–Uhlenbeck processes or even diffusion processes in general, but supports any (also not monotonically decreasing) variance schedules. In addition, the noise variances $\{\sigma_t\}_{t=0}^T$ are usually derived from the algorithm-internal parameters Θ that may include a noise-annealing schedule ($\{\alpha_t\}_{t=0}^T$ for C-DPS and DiffPIR and $\{\eta_t\}_{t=0}^T$ for DPnP).

Through this construction, DPS algorithms can use any statistic R of the samples $\{\bar{\mathbf{x}}_k\}_{k=1}^S$ in their update steps. Most methods use (possibly in addition to others) the mean $R(\bar{\mathbf{x}}_1, \dots, \bar{\mathbf{x}}_S) = \frac{1}{S} \sum_{k=1}^S \bar{\mathbf{x}}_k := \bar{\boldsymbol{\mu}}$, which is the Monte Carlo estimate of $\mathbb{E}[\mathbf{X}_0 | \mathbf{X}_t = \mathbf{x}_t]$. An example of a DPS algorithm that utilizes additional statistics is C-DPS that requires the Jacobian of $\mathbf{x}_t \mapsto \mathbb{E}[\mathbf{X}_0 | \mathbf{X}_t = \mathbf{x}_t]$. In settings where $(\mathbf{x}, t) \mapsto \mathbb{E}[\mathbf{X}_0 | \mathbf{X}_t = \mathbf{x}]$ is learned, the Jacobian is typically obtained by automatic differentiation. As we show in [appendix B](#), this Jacobian equals (up to the known VP scaling) the conditional covariance of $\mathbf{X}_0 | \mathbf{X}_t = \mathbf{x}_t$. In our framework, an unbiased estimator of the covariance matrix can be obtained through the statistic $R(\bar{\mathbf{x}}_1, \dots, \bar{\mathbf{x}}_S) = \frac{1}{S-1} \sum_{k=1}^S (\bar{\mathbf{x}}_k - \bar{\boldsymbol{\mu}})(\bar{\mathbf{x}}_s - \bar{\boldsymbol{\mu}})^T$. An example of a DPS algorithm that utilizes an alternative statistic is the DPnP algorithm that alternately samples a denoising problem and a data-proximal problem. There, the statistic $R(\bar{\mathbf{x}}_1, \dots, \bar{\mathbf{x}}_S) = \bar{\mathbf{x}}_1$ is used to obtain one sample from the denoising problem.

III. RELATED WORK

For unconditional generation, many works derive theoretical bounds on various distances between a target distribution and the distribution produced by (approximations of) the reverse SDE (12). These bounds relate the error to properties of the forward SDE, the target distribution, the score function, or the reverse-time discretization. For example, [48] contains bounds on the Wasserstein-2 distance with respect to the discretization error under the assumption that the target distribution is smooth and log-concave. These bounds translate directly to a bound

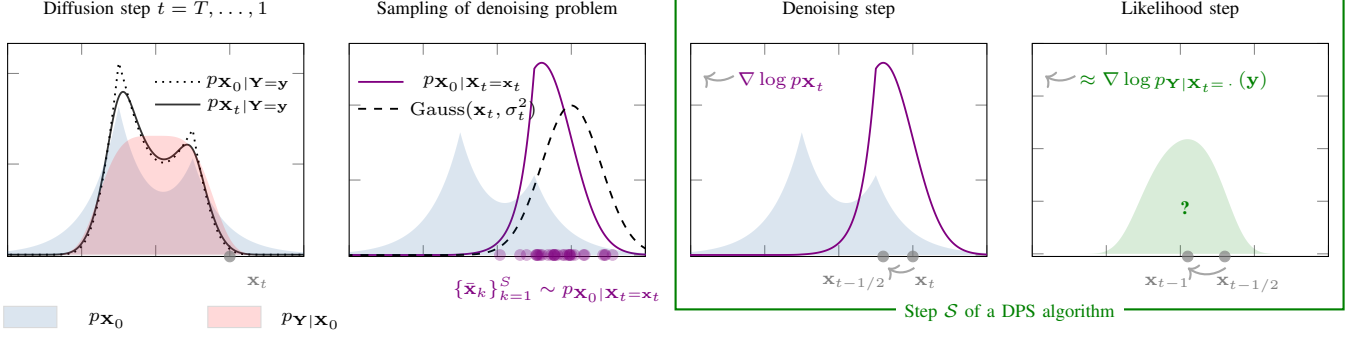


Fig. 3: Illustration of the proposed template for DPS algorithms. The benchmarked posterior sampler targets $\mathbf{x}_0 \sim p_{\mathbf{x}_0|\mathbf{Y}=\mathbf{y}}$ via a diffusion process. At each diffusion time t , first the samples $\{\bar{\mathbf{x}}_k\}_{k=1}^S \sim p_{\mathbf{x}_0|\mathbf{x}_t=\mathbf{x}_t}$ are drawn from the denoising posterior. Then, the step \mathcal{S} updates the iterate typically through a prior-guided update from the samples and a likelihood-guided update from the data. The likelihood guidance term is intractable and must be approximated, which constitutes the primary source of sampling error.

on the number of reverse-diffusion steps that is needed to obtain a desired accuracy. Under absolute continuity of the target with respect to a Gaussian, [49] gives bounds on the Kullback–Leibler divergence that depend on the noise schedule α . Additional results in total variation and other distances appear in the references cited therein.

A common simplification in analysis is to assume a Gaussian target. In that case, many objects in the forward and reverse SDE—including the posterior score $\nabla \log p_{\mathbf{x}_t|\mathbf{Y}=\mathbf{y}}$ for $t \geq 0$ —admit closed forms, which facilitates the computation of various bounds. For example, the authors of [50] analyze the effect of estimating the prior score (which is affine in this case) from finitely many samples of the target distribution and track the error propagation through the iterations of the reverse SDE. The authors of [22] derive explicit solutions to the SDE and use those to derive bounds on the Wasserstein-2 distance to the distributions that are obtained via the Euler–Maruyama discretizations.

The works that are closest to ours are [51] and [24]. The authors of [51] study posterior sampling with Gaussian priors theoretically. They derive expressions for the Wasserstein-2 distances between the conditional forward marginals (targets) and the distributions induced by specific likelihood approximations in the reverse SDE. Because their setting assumes Gaussian priors and Gaussian conditional likelihoods, all involved distributions are Gaussian,⁴ and the expression for the Wasserstein-2 distances are given by standard formulas that involve the covariance of the target distribution and the forward operator. Our framework is not restricted to Gaussian priors: we handle a broad family of priors that correspond to signals that are discretizations of Lévy processes (detailed next). Moreover, their framework targets algorithms that adhere to the strict likelihood-approximation structure that we detailed in section II-D, which many algorithms, *e.g.* DPnP, do not follow. Finally, although their expressions are explicit, deriving them for new algorithms often requires a substantial amount of nontrivial mathematics. In contrast, our benchmark and the

accompanying code are deliberately designed such that novel algorithms can be easily benchmarked, and additionally allows the quantification of the error that is incurred by substituting the optimal denoisers with their learned counterparts. The authors of [24] give a numerical evaluation of various DPS algorithms under the assumption of a (finite) Gaussian mixture prior. Similar to the present work, the authors provide reference objects to the DPS algorithm for a fair evaluation. However, their work is limited to the restrictive case of a Gaussian mixture prior which, as outlined in section I, cannot reproduce power-law-like extremes (heavy tails) and can overstate posterior quality.

Beyond diffusion-specific theory, the authors of [52] evaluate posterior calibration by checking coverage of credible regions produced by different Bayesian recovery strategies. They find that recovery strategies that utilize diffusion models often under-report uncertainty or, in other words, are overly confident. A shortcoming of their approach is that they use an empirical distribution of images as a surrogate for the prior distribution and, consequently, their approach is limited to the concrete application and dataset that is at hand. Our framework, by contrast, relies on known priors from which we can generate infinitely many signals and corresponding measurements. This isolates algorithmic error without resorting to surrogate priors and supports fair, repeatable comparisons across tasks and algorithms.

IV. PROPOSED FRAMEWORK

The prior distributions in our framework will be that of signals obtained by regularly spaced samples of processes with independent, stationary increments (Lévy processes and their discrete-time counterparts). We briefly recall the definition; see [53], [54] for background and the link to infinitely divisible laws.

Definition IV.1 (Lévy process). A stochastic process $s = \{s(t) : t \geq 0\}$ is a Lévy process if

- 1) $s(0) = 0$ almost surely;
- 2) (independent increments) for any $N \in \mathbb{N} \setminus \{0, 1\}$ and $0 \leq t_1 < t_2 < \dots < t_N < \infty$, the increments

⁴This also relies on the conditional likelihoods being Gaussian, which restricts their analysis to problems with Gaussian likelihoods and to those algorithms that adhere to the strict Bayesian structure described in section II-D.

$(s(t_2) - s(t_1)), (s(t_3) - s(t_2)), \dots, (s(t_N) - s(t_{N-1})))$ are mutually independent;

- 3) (stationary increments) for any given step h , the increment process $u_h = \{s(t) - s(t-h) : t > h\}$ is stationary;
- 4) (stochastic continuity) for any $\varepsilon > 0$ and $t \geq 0$

$$\lim_{h \rightarrow 0} \Pr(|s(t+h) - s(t)| > \varepsilon) = 0.$$

We form discrete signals by sampling s at integer times and stacking the values into $\mathbf{x} = (s(1), \dots, s(d))$. Let the unit-step increments be $\mathbf{u}_k = s(k) - s(k-1)$ for $k = 1, \dots, d$. By independence and stationarity, the law of \mathbf{u}_k does not depend on k and we denote it p_U .⁵ We define the finite-difference matrix

$$\mathbf{D} = \begin{bmatrix} 1 & 0 & 0 & \cdots & 0 \\ -1 & 1 & 0 & \cdots & 0 \\ 0 & -1 & 1 & \cdots & 0 \\ \vdots & \vdots & \ddots & \ddots & 0 \\ 0 & 0 & \cdots & -1 & 1 \end{bmatrix} \quad (26)$$

such that the increment vector satisfies

$$\mathbf{u} = \mathbf{D}\mathbf{x}. \quad (27)$$

Because $s(0) = 0$, \mathbf{D} is invertible and \mathbf{D}^{-1} is a lower-triangular matrix of ones, which also implies that for all $k = 1, 2, \dots, d$,

$$\mathbf{x}_k = \sum_{n=1}^k \mathbf{u}_n \quad (28)$$

which is a convenient way to synthesize signals once \mathbf{u} is drawn. The combination of (27) with the independence of the increments implies that the density of the discrete signal is

$$p_{\mathbf{X}}(\mathbf{x}) = \prod_{k=1}^d p_U((\mathbf{D}\mathbf{x})_k). \quad (29)$$

In this paper, we consider four increment families that are commonly used in sparse-process models: Gaussian, Laplace, Student-t, and Bernoulli–Laplace (spike-and-slab). We provide precise definitions and our notation of these and other distributions that we use in this work in [table V](#) in the appendix. Such increment laws yield sparse or heavy-tailed signals according to the taxonomy in [53] and are relevant in signal and image processing, finance, and many other fields [53], [55].

A. Efficient Posterior Sampling

The Bayesian treatment of the inverse problem in (1) yields the posterior

$$\begin{aligned} p_{\mathbf{X}|\mathbf{Y}=\mathbf{y}}(\mathbf{x}) &\propto \exp\left(-\frac{1}{2\sigma_n^2}\|\mathbf{A}\mathbf{x} - \mathbf{y}\|^2\right) p_{\mathbf{X}}(\mathbf{x}) \\ &= \exp\left(-\frac{1}{2\sigma_n^2}\|\mathbf{A}\mathbf{x} - \mathbf{y}\|^2\right) \prod_{k=1}^d p_U((\mathbf{D}\mathbf{x})_k). \end{aligned} \quad (30)$$

Unless p_U is a Gaussian (which is the simplified setting in [22]), this posterior is not conjugate, so neither closed-form sampling nor direct evaluation of moments is available. Nevertheless, for the increment laws used in this paper, the posterior distributions admit efficient Gibbs methods via standard latent-variable

Algorithm 2 Latent-variable Gibbs sampling of $p_{\mathbf{X}, \mathbf{Z}_1, \dots, \mathbf{Z}_N}$.

Require: Burn-in period $B \in \mathbb{N}$, number of samples $S \in \mathbb{N}$, initial point $(\mathbf{x}_0, \mathbf{z}_1, \dots, \mathbf{z}_N)$.

```

1: for  $s = 1, 2, \dots, B + S$  do
2:    $\mathbf{x}_s \sim p_{\mathbf{X}|\mathbf{Z}_1=\mathbf{z}_1, \dots, \mathbf{Z}_N=\mathbf{z}_N}$ 
3:    $\mathbf{z}_1 \sim p_{\mathbf{Z}_1|\mathbf{X}=\mathbf{x}_s, \dots, \mathbf{Z}_N=\mathbf{z}_N}$ 
4:    $\vdots$ 
5: return  $\{\mathbf{x}_{B+s}\}_{s=1}^S$ 

```

augmentations. Under these augmentations, all conditionals are either Gaussian or many independent one-dimensional distributions, both of which can be sampled efficiently, which results in rapidly mixing Gibbs methods. Such methods were recently shown to be significantly faster than other standard sampling routines that are commonly used in such settings in [56]. They report sampling efficiencies of close to 1, while alternatives, such as the Metropolis-adjusted Langevin algorithm, achieve sampling efficiencies of around 1×10^{-3} .⁶ In addition, Gibbs methods require no step-size or acceptance-rate tuning and introduce no discretization bias. These properties motivate our use of Gibbs methods for the fast and robust posterior sampling throughout this work.

1) Gibbs Methods: Gibbs methods are Markov chain Monte Carlo (MCMC) methods to sample from a joint distribution $p_{\mathbf{X}, \mathbf{Z}_1, \mathbf{Z}_2, \dots, \mathbf{Z}_N}$ of $(n+1)$ variables that are advantageous when the direct sampling is computationally difficult but sampling from the conditional distributions $p_{\mathbf{X}|\mathbf{Z}_1, \mathbf{Z}_2, \dots, \mathbf{Z}_N}, p_{\mathbf{Z}_1|\mathbf{X}, \mathbf{Z}_2, \dots, \mathbf{Z}_N}, \dots$ is easy. Gibbs methods cycle through the conditional distributions with repeated draws, which maintains the joint distribution invariant [58]. The naming of the variables $\mathbf{X}, \mathbf{Z}_1, \mathbf{Z}_2, \dots, \mathbf{Z}_N$ is deliberately chosen to emphasize that we use *latent-variable* Gibbs methods that rely on auxiliary variables that are introduced solely to make the conditionals simple. The steps of a general latent variable Gibbs sampler are shown in [algorithm 2](#), where the iteration counter in the sampling of the latent variables is omitted since they need not be stored and previous iterations can immediately be overwritten.

Like all MCMC methods, in practice Gibbs methods benefit from discarding some number of initial samples, the *burn-in period*, when the initial point is located in low-density regions. After the burn-in period, it is crucial to tune the number of samples such that the Monte Carlo estimates of various quantities, such as the MMSE estimate in (5), are sufficiently accurate. We discuss our choice of the burn-in period and the number of samples for the various problems in [section IV-B](#).

The Gaussian, Laplace, and Student-t distributions admit latent representations as infinite-component Gaussian mixture models, which makes them suitable for the Gaussian latent machine (GLM) framework that was recently introduced in [56]. The GLM framework is generally applicable to distributions

⁵For our choices, it always has a density w.r.t. a suitable reference measure.

⁶Sampling efficiency refers to effective samples per iteration; an efficiency of ρ means roughly $1/\rho$ iterations per “effective sample” [57, Section 11.5].

of the form

$$p_{\mathbf{X}}(\mathbf{x}) \propto \prod_{k=1}^n \phi_k((\mathbf{K}\mathbf{x})_k) \quad (31)$$

where $\mathbf{K} \in \mathbb{R}^{n \times d}$ and all distributions $\phi_1, \phi_2, \dots, \phi_n : \mathbb{R} \rightarrow \mathbb{R}$ have a latent representation

$$\phi_k(t) = \int_{\mathbb{R}} g_{\mu_k(z), \sigma_k^2(z)}(t) f_k(z) dz, \quad (32)$$

where the *latent distribution* f_i and the *latent maps* μ_i and σ_i^2 depend on the distribution ϕ_i and are tabulated in [table VI](#) for the distributions that are relevant in this paper.

The introduction of an appropriate n -dimensional random variable \mathbf{Z} with non-trivial distribution (see the details in [\[56\]](#)) enables the efficient sampling from the conditionals: Sampling $\mathbf{X} | \mathbf{Z} = \mathbf{z}$ amounts to sampling a Gaussian with covariance

$$\Sigma(\mathbf{z}) = (\mathbf{K}^T \Sigma_0(\mathbf{z})^{-1} \mathbf{K})^{-1} \quad (33)$$

and mean

$$\mu(\mathbf{z}) = \Sigma(\mathbf{z}) \mathbf{K}^T \Sigma_0(\mathbf{z})^{-1} \mu_0(\mathbf{z}) \quad (34)$$

where $\Sigma_0(\mathbf{z}) = \text{diag}(\sigma_1^2(\mathbf{z}_1), \sigma_2^2(\mathbf{z}_2), \dots, \sigma_n^2(\mathbf{z}_n))$ and $\mu_0(\mathbf{z}) = (\mu_1(\mathbf{z}_1), \mu_2(\mathbf{z}_2), \dots, \mu_n(\mathbf{z}_n))$. Sampling $\mathbf{Z} | \mathbf{X} = \mathbf{x}$ amounts to sampling n independent one-dimensional *conditional latent distributions* $p_{Z_i|X=(\mathbf{K}\mathbf{x})_i}$ that depend on the distributions ϕ_1, \dots, ϕ_n and are also given in [table VI](#).

The posterior distribution in [\(30\)](#) can be cast into this framework by rewriting it as

$$\begin{aligned} p_{\mathbf{X}|\mathbf{Y}=\mathbf{y}}(\mathbf{x}) &\propto \exp\left(-\frac{1}{2\sigma_n^2} \sum_{k=1}^m ((\mathbf{A}\mathbf{x})_k - \mathbf{y}_k)^2\right) \prod_{k=1}^d p_U((\mathbf{D}\mathbf{x})_k) \\ &\propto \prod_{k=1}^m g_{\mathbf{y}_k, \sigma_n^2}((\mathbf{A}\mathbf{x})_k) \prod_{k=1}^d p_U((\mathbf{D}\mathbf{x})_k) \\ &= \prod_{k=1}^{m+d} \phi_k((\mathbf{K}\mathbf{x})_k) \end{aligned} \quad (35)$$

by setting

$$\mathbf{K} = \begin{bmatrix} \mathbf{A} \\ \mathbf{D} \end{bmatrix} \quad (36)$$

and

$$\phi_k = \begin{cases} g_{\mathbf{y}_k, \sigma_n^2} & \text{for } k = 1, \dots, m, \\ p_U & \text{for } k = m+1, \dots, m+d. \end{cases} \quad (37)$$

We summarize the GLM sampling in [algorithm 3](#). It is easily adapted non-Gaussian likelihoods by substituting the respective first m distributions.

The Bernoulli–Laplace distribution requires the introduction of two latent variables to effectively handle the distribution of jumps due to the Bernoulli being “on” and the corresponding jump height that is distributed according to a Laplace distribution, and we use the algorithm that was proposed in [\[28\]](#). We start by noting that the Bernoulli–Laplace density

$$p_U(u) = \lambda \delta(u) + (1 - \lambda) \frac{b}{2} \exp(-b|u|) \quad (38)$$

Algorithm 3 GLM Gibbs sampler.

Require: Initial point $\mathbf{x}_0 \in \mathbb{R}^d$, operator $\mathbf{K} \in \mathbb{R}^{n \times d}$, distributions $\{\phi_i\}_{i=1}^n$ with corresponding conditional latent distributions $\{p_{Z_i|X}\}_{i=1}^n$ and latent maps $\{\mu_i, \sigma_i^2\}_{i=1}^n$

- 1: **for** $s = 1, \dots, B + S$ **do**
- 2: Draw $\mathbf{z}_i \sim p_{Z_i|X=(\mathbf{K}\mathbf{x}_{s-1})_i}$ \triangleright *par.* $i = 1, \dots, n$
- 3: Draw $\mathbf{x}_s \sim \text{Gauss}(\mu(\mathbf{z}), \Sigma(\mathbf{z}))$ \triangleright *see (33) and (34)*
- 4: **return** $\{\mathbf{x}_{B+s}\}_{s=1}^S$

with Bernoulli parameter λ and scale parameter b admits the representation

$$p_U(u) = \int_{\mathbb{R}} \left(\sum_{v=0}^1 p_{U|V=v, W=w}(u) p_V(v) \right) p_W(w) dw, \quad (39)$$

where

$$p_V(v) = \lambda^{1-v} (1 - \lambda)^v \quad (40)$$

for $v \in \{0, 1\}$ is a Bernoulli distribution,

$$p_W(w) = \frac{b^2}{2} \exp\left(-\frac{b^2 w}{2}\right) \chi_{\mathbb{R}_{\geq 0}}(w) \quad (41)$$

is an exponential distribution, and

$$p_{U|V=v, W=w}(u) = \begin{cases} \delta(u) & \text{if } v = 0, \\ \text{Gauss}(0, w) & \text{if } v = 1. \end{cases} \quad (42)$$

The algorithm relies on the introduction of two latent vectors $\mathbf{v}, \mathbf{w} \in \mathbb{R}^d$ that satisfy

$$p_{\mathbf{U}|\mathbf{V}=\mathbf{v}, \mathbf{W}=\mathbf{w}}(\mathbf{u}) = \prod_{k=1}^d p_{U|V=v_k, W=w_k}(\mathbf{u}_k) \quad (43)$$

such that, as a result, the distribution conditioned on the measurements can be written as

$$\begin{aligned} p_{\mathbf{U}, \mathbf{V}, \mathbf{W}|\mathbf{Y}=\mathbf{y}}(\mathbf{u}, \mathbf{v}, \mathbf{w}) &\propto \exp\left(-\frac{1}{2\sigma_n^2} \|\mathbf{H}\mathbf{u} - \mathbf{y}\|^2\right) \prod_{k=1}^d p_{U|V=v_k, W=w_k}(\mathbf{u}_k) \\ &\times \prod_{k=1}^d \lambda^{1-v_k} (1 - \lambda)^{v_k} \prod_{k=1}^d \frac{b^2}{2} \exp\left(-\frac{b^2 \mathbf{w}_k}{2}\right), \end{aligned} \quad (44)$$

where $\mathbf{H} = \mathbf{A}\mathbf{D}^{-1}$. [\(42\)](#) and [\(44\)](#) imply that any sample from $p_{\mathbf{U}|\mathbf{V}=\mathbf{v}, \mathbf{W}=\mathbf{w}, \mathbf{Y}=\mathbf{y}}$ takes the value zero at those indices where \mathbf{v} is zero, and values from a multivariate Gaussian distribution with covariance $\mathbf{C} = (\sigma_n^2 \mathbf{H}\mathbf{H}^T + \text{diag}(\mathbf{w}))^{-1}$ and mean $\sigma_n^{-2} \mathbf{C}\mathbf{H}^T \mathbf{y}$ otherwise. Sampling $\mathbf{W} | \mathbf{U} = \mathbf{u}, \mathbf{V} = \mathbf{v}, \mathbf{Y} = \mathbf{y}$ amounts to the independent sampling of d one-dimensional distributions, which are $\text{Exp}(2/b^2)$ at those indices where \mathbf{v} is zero and $\text{GIG}(b^2, \mathbf{u}_k^2, 0.5)$ those indices k where \mathbf{v} is one. The conditional distribution of the binary support vector is

$$\begin{aligned} p_{\mathbf{V}|\mathbf{W}=\mathbf{w}, \mathbf{Y}=\mathbf{y}}(\mathbf{v}) &\propto |\mathbf{B}(\mathbf{v}, \mathbf{w})|^{-\frac{1}{2}} \exp\left(-\frac{1}{2} \mathbf{y}^T \mathbf{B}(\mathbf{v}, \mathbf{w})^{-1} \mathbf{y}\right) \\ &\times \prod_{k=1}^d \lambda^{1-v_k} (1 - \lambda)^{v_k}, \end{aligned} \quad (45)$$

Algorithm 4 Bernoulli–Laplace Gibbs sampler.

Require: Initial jumps $\mathbf{u}_0 \in \mathbb{R}^n$

```

1: for  $s = 1, \dots, B + S$  do
2:   Draw  $\mathbf{w} \sim p_{\mathbf{W}} | \mathbf{U} = \mathbf{u}_{s-1}, \mathbf{V} = \mathbf{v}, \mathbf{Y} = \mathbf{y}$  ▷ see (44)
3:   for  $k = 1, \dots, d$  do
4:     Draw  $\mathbf{v}_k \sim \text{Bernoulli}(p_k)$  ▷ incremental, see (46)
5:     Draw  $\mathbf{u}_s \sim p_{\mathbf{U}} | \mathbf{V} = \mathbf{v}, \mathbf{W} = \mathbf{w}, \mathbf{Y} = \mathbf{y}$  ▷ see (44)
6: return  $\{\mathbf{D}^{-1} \mathbf{u}_{B+s}\}_{s=1}^S$ 

```

where $\mathbf{B}(\mathbf{v}, \mathbf{w}) = \sigma_n^2 \mathbf{I} + \mathbf{H} \text{diag}(\mathbf{v} \odot \mathbf{w}) \mathbf{H}^T$.⁷ The standard way to sample from this distribution is to use a coordinate-wise Gibbs sampler that updates $\mathbf{v}_k \sim \text{Bernoulli}(p_k)$ with

$$p_k = (1 + \exp(-\Delta_k))^{-1} \quad (46)$$

where the log-odds increment

$$\Delta_k = \log \frac{1-\lambda}{\lambda} - \frac{1}{2} (\log |\mathbf{B}(\mathbf{v}_{k=1}, \mathbf{w})| - \log |\mathbf{B}(\mathbf{v}_{k=0}, \mathbf{w})|) - \frac{1}{2} (\mathbf{y}^T \mathbf{B}(\mathbf{v}_{k=1}, \mathbf{w})^{-1} \mathbf{y} - \mathbf{y}^T \mathbf{B}(\mathbf{v}_{k=0}, \mathbf{w})^{-1} \mathbf{y}), \quad (47)$$

where $\mathbf{v}_{k= \cdot} := (\mathbf{v}_1, \dots, \mathbf{v}_{k-1}, \cdot, \mathbf{v}_{k+1}, \dots, \mathbf{v}_d)$ is the difference between the log-posterior when the bit is on and when it is off. This resulting algorithm, given in [algorithm 4](#), can be interpreted as $(d+2)$ -variable (*i.e.*, dimension-dependent) Gibbs method⁸ and an efficient implementation is crucial. We detail our implementation, which utilizes incremental updates of \mathbf{B} based on the Woodbury–Sherman–Morrison identities, in [section IV-B](#).

The Gibbs methods that we just described are suitable for the generation of the gold-standard samples of the posterior that corresponds to the initial inverse problem (1) as well as the generation of samples from the denoising problems that arise in the various DPS algorithms. For the latter, the forward operator \mathbf{A} is the identity, the measurements are the noisy intermediate reconstructions \mathbf{x}_t , and $\sigma_n = \sigma_t$ is the noise schedule at timestep t .

B. Benchmark Implementation Details

The benchmarking pipeline starts with the generation of N_{test} test signals denoted $\{\mathbf{x}_k^{\text{test}}\}_{k=1}^{N_{\text{test}}}$ per jump distribution, each of which is independently synthesized by first drawing i.i.d. increments from the respective jump distribution and forming the signals via (28). It then proceeds to synthesize the N_{test} measurements (*i.e.* we use one noise instance per signal) denoted $\{\mathbf{y}_k^{\text{test}}\}_{k=1}^{N_{\text{test}}}$ according to (1) and, for each of the measurements, computes the gold-standard posterior samples of the various inverse problems via the Gibbs methods described in [section IV-A](#). This stage is off-line (no reverse-diffusion loop) and trivially parallel across the measurements, which allows us to run long chains with burn-in periods of

⁷This is a different but equivalent formulation to what is presented in [28], where the authors explicitly “slice” the matrices \mathbf{H} and $\text{diag}(\mathbf{w})$ with the indices where \mathbf{v} is one. We stick to this formulation since it requires less notation and emphasizes that implementations need not build variable-sized matrices, which is crucial for an efficient implementation on modern compute units that utilize highly parallelized computations.

⁸This is not strictly correct since the density violates the classical positivity conditions that are needed for Gibbs methods. It is a *partially collapsed* Gibbs method, see [28], [59].

1×10^5 iterations and obtain 2×10^5 draws from the posterior distribution. This far exceeds any values reported in [56] or [28] and results in precise MMSE estimates.

The dataset generation stage also involves the generation of N_{train} training signals $\{\mathbf{x}_k^{\text{train}}\}_{k=1}^{N_{\text{train}}}$ and N_{val} validation signals (mutually disjoint from the test signals) $\{\mathbf{x}_k^{\text{val}}\}_{k=1}^{N_{\text{val}}}$ and the corresponding validation measurements $\{\mathbf{y}_k^{\text{val}}\}_{k=1}^{N_{\text{val}}}$. The training signals are used for the learning of a neural score function like those that are used for the resolution of inverse problems when the prior is unknown or too expensive to evaluate. The validation signals are used to monitor the performance of the neural score function on unseen signals during the training stage and to tune the regularization parameters for the model-based approaches as well as the parameters of the DPS algorithms, see [section V-B1](#) and [section V-B2](#).

Unlike for the computation of the gold-standard MMSE estimate of the initial inverse problem, the denoising posteriors are sampled T times per trajectory (we use $T = 1000$). To ensure acceptable runtimes in this setting, we therefore pick the smallest burn-in period and sample count that still yield accurate estimates of the required statistics. We determine these settings with a rigorous protocol that is detailed in [appendix C](#). Ultimately, this protocol resulted in the choice of a burn-in period of 100 iterations and a sample count of 300.

1) Practical Gibbs Implementations: Sampling $\mathbf{X} | \mathbf{Z}$ in the GLM and $\mathbf{U} | \mathbf{V}, \mathbf{W}, \mathbf{Y}$ for the Bernoulli–Laplace case reduces to drawing from a high-dimensional Gaussian, which is a well-studied problem. For settings that necessitate a matrix-free implementation such as those that are commonly encountered in imaging applications, the authors of [56] advocate a Perturb-and-MAP sampler with preconditioned conjugate gradient solvers. For our moderate-dimensional problems with $d = 64$, a standard implementation based on the Cholesky factorization of the covariance matrix offered significantly faster (approximately one order of magnitude) sampling. The sampling of the different latent variables necessitates the sampling of the one-dimensional conditional latent distributions. All the conditional latent distributions that are relevant in this paper admit efficient samplers that are readily available in standard scientific computing packages or can be implemented with little effort. We reuse the CUDA implementation of the generalized inverse Gaussian sampler from [56] that implements the method proposed in [60] and rely on `pytorch` [61] for all others. Wherever possible, latent updates are parallelized.

In the Gibbs methods for the Bernoulli–Laplace jumps, the sequential drawing of the binary support vector \mathbf{V} is embedded in the outer Gibbs loop, which, in turn, may be embedded in the reverse-diffusion loop. This makes it crucial to minimize the use of heavy linear algebra operations to achieve acceptable runtimes. Writing $\mathbf{B}(\mathbf{v}, \mathbf{w}) = \sigma_n^2 \mathbf{I} + \mathbf{H} \text{diag}(\mathbf{v} \odot \mathbf{w}) \mathbf{H}^T$, we recognize that flipping the k th bit of \mathbf{v} adds or removes a rank-one term $\mathbf{w}_k \mathbf{H}_k \mathbf{H}_k^T$, where \mathbf{H}_k is the k th column of \mathbf{H} . Using the matrix determinant lemma and Woodbury–Sherman–Morrison, we update

$$\log |\mathbf{B}(\mathbf{v}_{k=1}, \mathbf{w})| = \log |\mathbf{B}(\mathbf{v}_{k=0}, \mathbf{w})| + \log(1 + \mathbf{w}_k \tau_k) \quad (48)$$

and

$$\mathbf{y}^T \mathbf{B}(\mathbf{v}_{k=1}, \mathbf{w})^{-1} \mathbf{y} = \mathbf{y}^T \mathbf{B}(\mathbf{v}_{k=0}, \mathbf{w})^{-1} \mathbf{y} - \frac{\mathbf{w}_k (\mathbf{H}_k^T \mathbf{B}(\mathbf{v}_{k=0}, \mathbf{w})^{-1} \mathbf{y})^2}{1 + \mathbf{w}_k \tau_k}, \quad (49)$$

where $\tau_k = \mathbf{H}_k^T \mathbf{B}(\mathbf{v}_{k=0}, \mathbf{w})^{-1} \mathbf{H}_k$. Thus, an efficient implementation factors $\mathbf{B}(\mathbf{v}, \mathbf{w})$ once per latent state, obtains the needed scalars via triangular solves, and performs rank-one updates as bits flip.

V. NUMERICAL EXPERIMENTS

A. Forward Operators

We consider four forward operators that are frequently encountered in various estimation tasks throughout the natural sciences. First, the identity $\mathbf{A} = \mathbf{I} \in \mathbb{R}^{d \times d}$. This choice is motivated by the fundamental role that denoising algorithms currently play in many restoration algorithms and even labeling problems such as edge detection [62]. Second, a convolution operator $\mathbf{A} \in \mathbb{R}^{d \times d}$ that implements the convolution with a kernel that consists of the 13 central samples of a truncated Gaussian with variance 2 and is normalized to unit sum. We adopt circular boundary conditions to enable a fast computation of the proximal map that arises in the update step of DiffPIR (see table I) via the fast Fourier transform. Deconvolution is a relevant problem with applications in, *e.g.*, microscopy and astronomy. Third, a sampling operator $\mathbf{A} \in \mathbb{R}^{m \times d}$ that returns $m < d$ entries of its argument unchanged. This operator is also relevant in many fields such as image reconstruction and time-series forecasting. In particular, a forecasting or prediction problem can be modeled by returning the first m known entries recovering the remaining $(d-m)$ entries through the resolution of the inverse problem. In our experiments, each entry has an independent chance of 40% being kept. Fourth, an operator $\mathbf{A} = \mathbf{M}\mathbf{F} \in \mathbb{R}^{m \times d}$ where $\mathbf{F} \in \mathbb{R}^{2(\lfloor d/2 \rfloor + 1) \times d}$ is the matrix representation of the “real” one-dimensional discrete Fourier transform with separated real and imaginary components, and $\mathbf{M} \in \mathbb{R}^{m \times 2(\lfloor d/2 \rfloor + 1)}$ is a sampling operator. Such operators are relevant in, *e.g.*, medical imaging and astronomy. The sampling operator is constructed such that the 5 lowest frequencies (including the DC term) are acquired, and the remaining frequencies independently have a 40% chance of being kept.

For all operators, the noise variance σ_n^2 is chosen such that the median measurement signal-to-noise ratio (SNR) is around 25 dB. We set $N_{\text{train}} = 1 \times 10^6$, $N_{\text{val}} = 1 \times 10^3$, and $N_{\text{test}} = 1 \times 10^3$.

B. Reconstruction Algorithms

We now describe the reconstruction algorithms that we compare and how we obtain suitable parameters. For the sake of simplicity, the parameter estimation procedures are given for a general jump distribution and forward operator. The parameters are estimated independently for each jump distribution and forward operator.

1) *Model-Based Methods*: As baseline reconstruction algorithms we consider the model-based methods

$$\hat{\mathbf{x}}^{\ell_2}(\mathbf{y}, \lambda) = \arg \min_{\mathbf{x} \in \mathbb{R}^d} \left(\frac{1}{2} \|\mathbf{A}\mathbf{x} - \mathbf{y}\|^2 + \lambda \|\mathbf{D}\mathbf{x}\|^2 \right), \quad (50)$$

and

$$\hat{\mathbf{x}}^{\ell_1}(\mathbf{y}, \lambda) = \arg \min_{\mathbf{x} \in \mathbb{R}^d} \left(\frac{1}{2} \|\mathbf{A}\mathbf{x} - \mathbf{y}\|^2 + \lambda \|\mathbf{D}\mathbf{x}\|_1 \right), \quad (51)$$

which coincide with the MAP estimators of Lévy processes associated with Laplace Gaussian and Laplace distributions, respectively. The adjustable regularization parameter for the method $\text{est} = \ell_2, \ell_1$ was found by

$$\lambda^{\text{est},*} = \arg \min_{\lambda \in \Lambda} \frac{1}{N_{\text{val}}} \sum_{k=1}^{N_{\text{val}}} \frac{1}{d} \|\hat{\mathbf{x}}^{\text{est}}(\mathbf{y}_k^{\text{val}}, \lambda) - \mathbf{x}_k^{\text{val}}\|^2, \quad (52)$$

where Λ is a finite set of real numbers. Λ is detailed appendix D and the obtained MSE curves are shown in fig. 7.

2) *Diffusion Posterior Sampling Algorithms*: We consider three DPS algorithms that are popular in the literature. First, the C-DPS algorithm due to Chung et al. [38], which was one of the first algorithms that was proposed for the resolution of general noisy inverse problems with diffusion priors. Second, the DiffPIR algorithm due to Zhu et al. [46] that can be regarded as an extension of the C-DPS algorithm and typically reports superior results in standard perception-based evaluations. Third, the DPnP algorithm due to Xu et al. [29] that alternates between sampling the denoising subproblem and a data-proximal subproblem. We include the DPnP algorithm to showcase the broad applicability of our framework to nonstandard setups that utilize various statistics of the denoising problem.

For each DPS algorithm, we benchmark two variants: One where the sampling of the denoising problem is done with the gold-standard Gibbs methods (“oracle” denoiser) and statistics are computed from those samples, and one where the sampling (or the direct estimation of any point estimate) is done with learned components. For the second case, a noise-conditional neural network with UNet architecture (305 761 learnable parameters) is trained in an off-line step on the N_{train} training signals in a standard setup (Adam optimizer with learning rate 1×10^{-4} with exponential decay with factor 0.9999, 100 000 parameter updates, batch size 10 000). The noise schedule in C-DPS and DiffPIR is defined by the two endpoints $\beta_0 = 1 \times 10^{-4}$ and $\beta_T = 2 \times 10^{-2}$ with linear equidistant samples in-between. The learned variant of DPnP is the “DDS-DDPM” variant [29, Algorithms 1 and 3] that contains an inner denoising-sampling loop. The oracle variant does not require an inner loop at all (except for the burn-in period), which makes the oracle variant the faster one for this case.

Before advancing, we introduce some notation. For any given measurements \mathbf{y} , any DPS algorithm alg that depends on any parameters $\boldsymbol{\theta}$ produces samples denoted $\{\hat{\mathbf{x}}_k^{\text{alg}}(\mathbf{y}, \boldsymbol{\theta})\}_{k=1}^{N_{\text{samples}}}$. We denote $\hat{\mathbf{x}}_{\text{MMSE}}^{\text{alg}}(\mathbf{y}, \boldsymbol{\theta}) := \frac{1}{N_{\text{samples}}} \sum_{k=1}^{N_{\text{samples}}} \hat{\mathbf{x}}_k^{\text{alg}}(\mathbf{y}, \boldsymbol{\theta})$. We tune the parameters of the methods by finding

$$\boldsymbol{\theta}^{\text{alg},*} = \arg \min_{\boldsymbol{\theta} \in \Theta^{\text{alg}}} \sum_{k=1}^{N_{\text{val}}} \|\hat{\mathbf{x}}_{\text{MMSE}}^{\text{alg}}(\mathbf{y}_k^{\text{val}}, \boldsymbol{\theta}) - \mathbf{x}_k^{\text{val}}\|^2 \quad (53)$$

| C-DPS | DiffPIR | DPnP |
|---|---|---|
| $\Theta = \{(1 - \bar{\alpha}_t)/\bar{\alpha}_t\}_{t=1}^T, \zeta$ | $\Theta = \{(1 - \bar{\alpha}_t)/\bar{\alpha}_t\}_{t=1}^T, \lambda, \zeta$ | $\Theta = \{\eta_t\}_{t=1}^T$ |
| $\hat{\mathbf{x}}_0 = \frac{1}{S} \sum_{k=1}^S \bar{\mathbf{x}}_k$ | $\hat{\mathbf{x}}_0 = \frac{1}{S} \sum_{k=1}^S \bar{\mathbf{x}}_k$ | |
| $\mathbf{C} = \frac{1}{S} \sum_{k=1}^S (\bar{\mathbf{x}}_k - \hat{\mathbf{x}}_0)(\bar{\mathbf{x}}_k - \hat{\mathbf{x}}_0)^T$ | $\rho_t = \lambda \sigma_n^2 / \sigma_t^2$ | $\mathbf{x}_0 = \bar{\mathbf{x}}_1$ |
| $\mathbf{x}'_{t-1} = \frac{\sqrt{\bar{\alpha}_t}(1 - \bar{\alpha}_{t-1})}{1 - \bar{\alpha}_t} \mathbf{x}_t + \frac{\sqrt{\bar{\alpha}_{t-1}}\beta_t}{1 - \bar{\alpha}_t} \hat{\mathbf{x}}_0 + \sigma_t z$ | $\bar{\mathbf{x}}_0 = \arg \min_{\mathbf{x}} \left(\frac{1}{2} \ \mathbf{A}\mathbf{x} - \mathbf{y}\ ^2 + \frac{\rho_t}{2} \ \mathbf{x} - \hat{\mathbf{x}}_0\ ^2 \right)$ | $\mathbf{x}_{t-1} \sim \exp\left(-\frac{1}{2} \ \mathbf{A} \cdot -\mathbf{y}\ ^2 - \frac{1}{2\eta_t^2} \ \cdot - \mathbf{x}_0\ ^2\right)$ |
| $\mathbf{x}_{t-1} = \mathbf{x}'_{t-1} - \zeta_t \frac{\sqrt{\bar{\alpha}_t}}{1 - \bar{\alpha}_t} \mathbf{C}^T \mathbf{A}^T (\mathbf{A}\hat{\mathbf{x}}_0 - \mathbf{y})$ | $\hat{\epsilon} = \frac{1}{\sqrt{1 - \bar{\alpha}_t}} (\mathbf{x}_t - \sqrt{\bar{\alpha}_t} \bar{\mathbf{x}}_0)$ | |
| $\mathbf{x}_{t-1} = \mathbf{x}'_{t-1} - \zeta_t \frac{\sqrt{\bar{\alpha}_t}}{1 - \bar{\alpha}_t} \mathbf{C}^T \mathbf{A}^T (\mathbf{A}\hat{\mathbf{x}}_0 - \mathbf{y})$ | $\mathbf{x}'_{t-1} = \sqrt{\bar{\alpha}_{t-1}} \bar{\mathbf{x}}_0 + \sqrt{1 - \bar{\alpha}_{t-1}} (\sqrt{1 - \zeta} \hat{\epsilon} + \sqrt{\zeta} z)$ | |
| $\mathbf{x}_{t-1} = \mathbf{x}'_{t-1} / \sqrt{\bar{\alpha}_{t-1}}$ | $\mathbf{x}_{t-1} = \mathbf{x}'_{t-1} / \sqrt{\bar{\alpha}_{t-1}}$ | |

TABLE I: Instantiations of the update step $\mathcal{S}(\mathbf{x}_t, \{\bar{\mathbf{x}}_k\}_{k=1}^S, \mathbf{y}, \mathbf{A}, \Theta, t)$ and description of the algorithm parameters Θ for C-DPS, DiffPIR, and DPnP. Each z is a d -dimensional random vector with i.i.d. standard Gaussian entries.

where the grid Θ^{alg} is method-dependent. Note that this tuning is specifically tailored towards the evaluation with respect to the MMSE optimality gap. Due to resource constraints, the parameters are tuned for the learned denoiser. The parameter grids for the different methods is detailed in [appendix D](#) and the corresponding MSE curves are shown in [fig. 7](#). We use $N_{\text{samples}} = 10$ for the grid search on the validation set and $N_{\text{samples}} = 50$ for the experiments on the test set.

3) *Gold-Standard Gibbs Methods*: The Gibbs methods are used to obtain gold-standard samples from the posterior. As described in [section IV-A](#), the Gibbs methods are parameter-free and efficient and, consequently, well-suited for this purpose. Chain lengths, diagnostics, and implementation details are given in [section IV-B](#); we reuse the same settings across operators and increment families.

C. Results

For a method est and test data $\mathbf{y}_k^{\text{test}}$ with corresponding data-generating signal $\mathbf{x}_k^{\text{test}}$ we measure the MMSE optimality gap (in decibel) defined by

$$10 \log_{10} \left(\frac{\|\hat{\mathbf{x}}^{\text{est}}(\mathbf{y}_k^{\text{test}}) - \mathbf{x}_k^{\text{test}}\|^2}{\|\hat{\mathbf{x}}_{\text{MMSE}}^{\text{Gibbs}}(\mathbf{y}_k^{\text{test}}) - \mathbf{x}_k^{\text{test}}\|^2} \right) \quad (54)$$

where $\hat{\mathbf{x}}^{\text{est}}(\mathbf{y}) = \hat{\mathbf{x}}^{\text{est}}(\mathbf{y}, \lambda^{\text{est},*})$ for model-based methods and $\hat{\mathbf{x}}_{\text{MMSE}}^{\text{est}}(\mathbf{y}, \theta^{\text{est},*})$ for DPS algorithms. The MMSE optimality gap shows the degree of optimality of a method at a glance without the need to compare to a reference: A gap of 0 indicates a perfect recovery of the gold-standard MMSE estimate and the positive nonzero values show the orders of magnitude of the error relative to the reference error.

We report the mean and standard deviation of the MMSE optimality gap defined in (54) for the learned denoiser over the entire test set in [table II](#). The Gaussian jump distribution validates the implementation: Since the MMSE and the MAP point estimates coincide, the model-based ℓ_2 estimator matches the Gibbs reference up to the error due to the finite grid resolution. When the posterior mean is smooth (e.g., imputation and some deconvolution cases), ℓ_2 is the best model-based choice and frequently beats the DPS algorithms. When the posterior mean is (close to) piecewise constant (typical in denoising of signals with sparse jumps), the ℓ_1 estimator is preferred. Among DPS algorithms, DiffPIR is typically the top

performer and exceeds ℓ_2 and ℓ_1 baselines in deconvolution, imputation, and reconstruction from partial Fourier measurements. For spike-and-slab settings (Bernoulli–Laplace), DPS algorithms substantially outperform the model-based baselines across operators. In deconvolution, and reconstruction from partial Fourier measurements, DPS algorithms frequently match or surpass the best model-based estimator, with DPnP and DiffPIR alternating as the strongest.

In addition to the reconstruction performance obtained with the learned denoisers—for which the parameters of the algorithms were tuned—we inspect the robustness of the algorithms when substituting the learned denoiser with the oracle denoiser by reporting the difference in the MMSE optimality gap between the two in [table III](#). DPnP is the most robust to swapping the learned denoiser with the oracle denoiser. Indeed, DPnP significantly benefits from the oracle denoiser in the most challenging cases of the spike-and-slab prior and the extremely heavy-tailed t-distribution with degree of freedom parameter $\nu = 1$. By contrast, C-DPS and DiffPIR can require retuning when the denoiser changes. This sensitivity is most visible under heavy-tailed jumps (e.g., St(1) jumps): reusing hyperparameters tuned on the learned denoiser can degrade scores for the oracle denoiser (see, e.g., deconvolution and imputation for BL(0.1, 1) and St(1)), whereas a brief hand-tuning on the validation set improves DiffPIR way beyond the learned denoiser (e.g., $\zeta = 0.7$ and $\rho = 4$ decreased the optimality gap by almost 10 dB). We did not exhaustively retune all methods for the oracle denoiser due to resource limits; the framework supports this, and we view full oracle-side tuning as a community task. [Table III](#) also reports for which cases the oracle denoiser reports significantly better results than the learned denoiser according to a Wilcoxon signed-rank test ($p = 0.05$, N_{test} pairs, two-sided test with the winner determined by the median of differences). The differences between the algorithms are generally greater than the differences between the learned/oracle variants except for the heavy-tailed cases, which confirms the findings in [\[28\]](#) and indicates that the research of efficient and robust DPS algorithms is still crucial.

Uncurated examples of the MMSE estimates and the marginal variances obtained by the DPS algorithms and the gold-standard Gibbs methods for deconvolution with the oracle

| | | Gauss(0.25) | Laplace(1) | BL(0.1, 1) | St(1) | St(2) | St(3) |
|---------------|---------|-------------|------------|-------------|-------------|------------|------------|
| Denoising | C-DPS | 0.12± 0.18 | 0.12± 0.20 | 2.22± 2.26 | 3.26± 1.01 | 0.28± 0.30 | 0.10± 0.18 |
| | DiffPIR | 0.16± 0.21 | 0.09± 0.16 | 0.72± 1.10 | 0.93± 1.06 | 0.07± 0.14 | 0.15± 0.21 |
| | DPnP | 0.24± 0.25 | 0.11± 0.17 | 1.33± 2.12 | 1.19± 1.38 | 0.10± 0.17 | 0.10± 0.17 |
| | L1 | 0.15± 0.21 | 0.06± 0.12 | 3.44± 2.38 | 0.38± 0.43 | 0.14± 0.19 | 0.11± 0.18 |
| | L2 | 0.00± 0.01 | 0.16± 0.21 | 8.61± 3.10 | 3.25± 0.99 | 0.74± 0.83 | 0.25± 0.33 |
| Deconvolution | C-DPS | 0.12± 0.20 | 0.12± 0.23 | 4.30± 3.87 | 18.30± 5.28 | 0.46± 1.40 | 0.17± 0.53 |
| | DiffPIR | 0.07± 0.17 | 0.07± 0.19 | 1.09± 2.22 | 10.45± 6.10 | 0.09± 0.57 | 0.08± 0.26 |
| | DPnP | 0.10± 0.18 | 0.13± 0.22 | 1.71± 2.49 | 7.84± 5.66 | 0.35± 1.39 | 0.14± 0.41 |
| | L1 | 1.65± 0.84 | 1.38± 0.86 | 1.86± 3.14 | 1.87± 4.01 | 1.10± 1.19 | 1.28± 0.94 |
| | L2 | 0.00± 0.01 | 0.07± 0.23 | 6.11± 4.49 | 21.50± 4.46 | 1.44± 2.85 | 0.36± 1.09 |
| Imputation | C-DPS | 0.15± 0.29 | 0.18± 0.39 | 2.99± 2.82 | 23.33± 8.69 | 0.50± 1.09 | 0.14± 0.57 |
| | DiffPIR | 0.09± 0.23 | 0.08± 0.24 | 0.24± 1.14 | 0.88± 3.50 | 0.11± 0.62 | 0.08± 0.42 |
| | DPnP | 0.14± 0.32 | 0.17± 0.36 | 0.50± 1.28 | 10.89± 5.92 | 0.25± 0.82 | 0.27± 0.58 |
| | L1 | 1.74± 1.12 | 1.77± 1.35 | 1.25± 2.78 | 13.32± 5.32 | 1.37± 2.56 | 1.55± 1.58 |
| | L2 | 0.00± 0.01 | 0.01± 0.05 | 1.10± 1.88 | 0.42± 0.95 | 0.06± 0.34 | 0.02± 0.28 |
| Fourier | C-DPS | 0.15± 0.36 | 0.26± 0.65 | 5.90± 4.41 | 4.29± 5.78 | 0.53± 0.83 | 0.35± 0.77 |
| | DiffPIR | 0.11± 0.29 | 0.08± 0.31 | 0.83± 1.44 | 3.19± 4.37 | 0.11± 0.39 | 0.12± 0.37 |
| | DPnP | 0.11± 0.35 | 0.20± 0.51 | 1.88± 2.47 | 2.45± 4.83 | 0.39± 0.89 | 0.24± 0.64 |
| | L1 | 1.50± 1.59 | 0.73± 0.94 | 3.57± 2.82 | 1.07± 2.98 | 0.71± 0.99 | 0.78± 0.97 |
| | L2 | 0.00± 0.02 | 0.36± 0.73 | 12.22± 4.53 | 9.47± 8.34 | 2.66± 3.57 | 1.03± 1.79 |

TABLE II: MMSE optimality gap in decibel (mean \pm standard deviation; lower is better; 0 is a perfect reconstruction) of various estimation methods over the test set.

| | | Gauss(0.25) | Laplace(1) | BL(0.1, 1) | St(1) | St(2) | St(3) |
|---------------|---------|-------------|--------------|--------------|---------------|--------------|-------------|
| Denoising | C-DPS | 0.00± 0.11 | 0.00± 0.16 | -0.46± 1.16* | 0.00± 0.01 | 0.02± 0.79* | -0.01± 0.14 |
| | DiffPIR | 0.00± 0.13 | 0.00± 0.17 | -0.05± 0.78* | -0.41± 0.80* | 0.00± 0.20 | 0.00± 0.15 |
| | DPnP | 0.04± 0.27* | -0.01± 0.22 | -0.55± 1.31* | -0.77± 1.31* | 0.00± 0.24 | 0.00± 0.23 |
| Deconvolution | C-DPS | -0.01± 0.24 | 0.00± 0.26 | 0.09± 0.97* | 6.64± 3.21* | -0.12± 1.11* | -0.03± 0.43 |
| | DiffPIR | -0.01± 0.23 | 0.00± 0.23 | 0.04± 1.12 | 13.56± 9.90* | -0.01± 0.47 | 0.00± 0.31 |
| | DPnP | 0.00± 0.25 | -0.01± 0.27* | -0.02± 1.20 | -4.98± 3.86* | 0.06± 0.77 | -0.02± 0.34 |
| Imputation | C-DPS | 0.00± 0.30 | 0.01± 0.35 | 0.41± 1.51* | 3.41± 4.99* | -0.12± 1.01* | -0.01± 0.57 |
| | DiffPIR | 0.00± 0.29 | 0.00± 0.33 | 0.03± 1.05 | -0.20± 3.05* | 0.03± 0.71 | 0.00± 0.47 |
| | DPnP | 0.00± 0.35 | -0.02± 0.38 | -0.02± 1.02 | -10.46± 5.70* | 0.02± 0.67 | -0.01± 0.48 |
| Fourier | C-DPS | -0.02± 0.43 | -0.01± 0.49 | 0.80± 1.43* | 0.09± 5.63* | -0.03± 0.79* | 0.01± 0.49 |
| | DiffPIR | -0.01± 0.39 | 0.00± 0.40 | 0.12± 0.83* | -0.64± 1.70* | -0.03± 0.42* | -0.02± 0.38 |
| | DPnP | -0.01± 0.43 | 0.00± 0.45 | -0.33± 1.13* | -1.32± 3.18* | 0.00± 0.54 | 0.01± 0.46 |

TABLE III: Change in MMSE optimality gap (mean \pm standard deviation) after substituting the learned denoiser with the oracle denoiser. An asterisk indicates a significant changes according to a Wilcoxon signed-rank test ($p = 0.05$): Negative number with asterisk: oracle denoiser is significantly better; positive number with asterisk: learned denoiser is significantly better.

denoiser for BL(0.1, 1), St(1), St(2), and Laplace(1) jump distributions are shown in [fig. 4](#). The learned counterpart and the results for denoising, imputation, and reconstruction from partial Fourier measurements are provided in [figs. 10 to 16](#). In all of those figures, we deliberately omit the underlying signal to emphasize that the targets are the MMSE estimate and the marginal variance that are obtained by the gold-standard Gibbs methods.

[Figure 9](#) shows a typical conditional reverse-diffusion trajectory (here obtained by DiffPIR for deconvolution and a BL(0.1, 1) jump distribution) that highlights a key distinction: Posterior *samples* often preserve high-frequency structure and reflect prior variability, whereas the *MMSE point estimate*—obtained by averaging all samples—is much smoother. This explains why DPS methods tend to score higher on preception-oriented metrics, while regressors trained with an MSE loss target the MMSE and therefore excel on metrics distortion metrics (e.g., peak signal-to-noise-ratio (PSNR), MSE). Consistent with this distinction, [\[44\]](#) fairly compare a sampling-based

method to an MMSE regressor and find the expected trade-off: higher PSNR and structural similarity (SSIM) for the regressor and better perceptual scores for the sampler. We therefore recommend making the Bayesian target explicit—point estimate versus sample quality—and using evaluation protocols that are aligned to that target. Our framework supports this by offering gold-standard posterior samples and oracle denoisers.

In addition to the evaluation of the MMSE optimality gap, which is on the point-estimator level, we analyze the high-posterior density coverage of the algorithms. Specifically, for any datum \mathbf{y} and any $k = 1, \dots, N_{\text{samples}}$, denote $l_k(\mathbf{y}) := \log p_{\mathbf{x}|\mathbf{Y}=\mathbf{y}}(\hat{\mathbf{x}}_{P(k)}^{\text{alg}}(\mathbf{y}, \boldsymbol{\theta}^{\text{alg},*}))^9$ where P is the permutation that ensures that $l_1(\mathbf{y}) \geq l_2(\mathbf{y}) \geq \dots \geq l_{N_{\text{samples}}}(\mathbf{y})$ and define the empirical highest-posterior-density threshold at $\alpha \in [0, 1]$ as $l_{\lceil \alpha N_{\text{samples}} \rceil}(\mathbf{y})$. We declare the data-generating signal \mathbf{x}

⁹With slight abuse of notation, $\log p_{\mathbf{x}|\mathbf{Y}=\mathbf{y}}$ is the unnormalized ground-truth log-posterior [\(30\)](#); the additive constant is the same across all methods so ranking is valid.

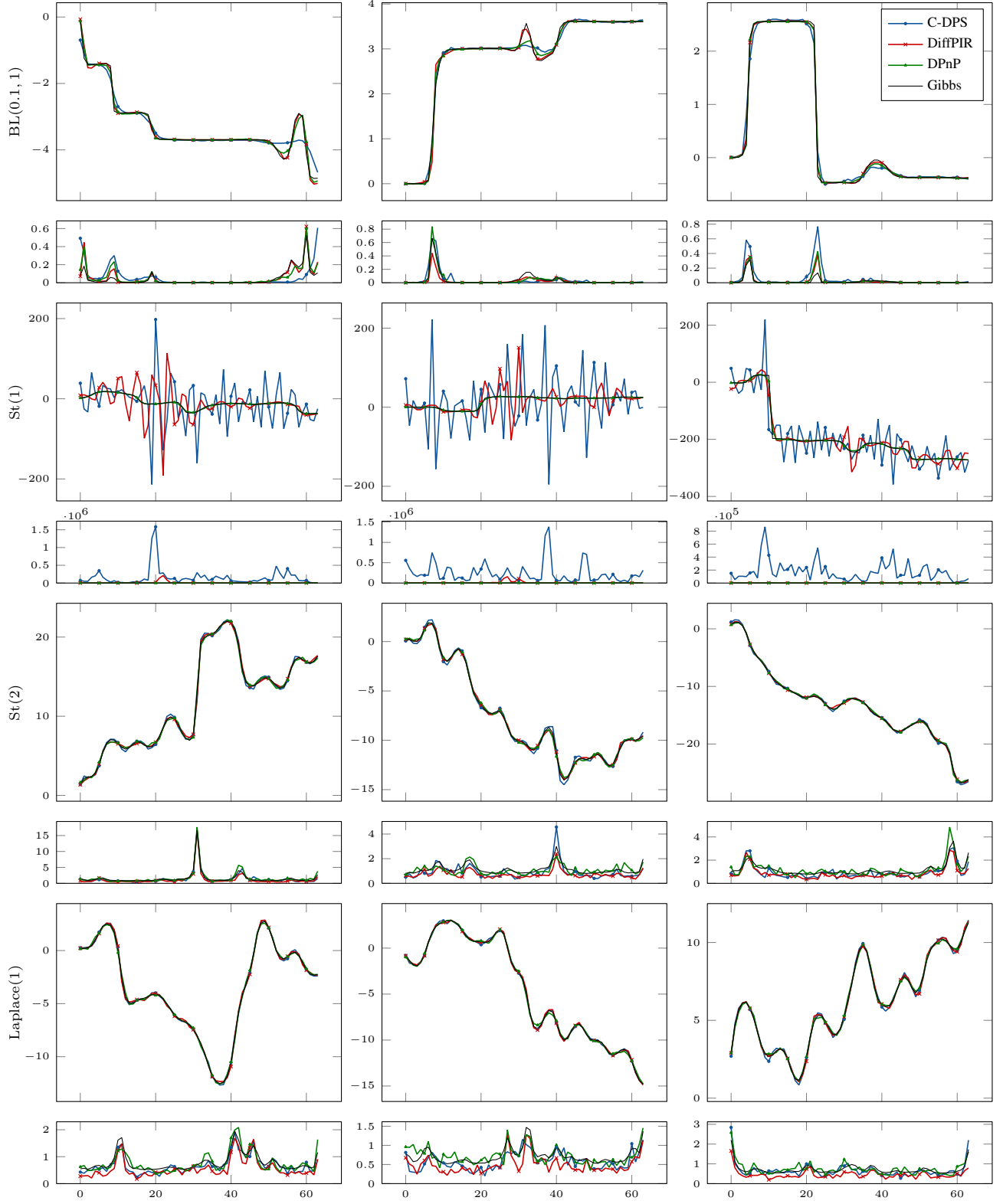


Fig. 4: Qualitative results for deconvolution using the oracle denoising sampler. Rows: Jump distributions. For each jump distribution, the MMSE estimates obtained by the different DPS algorithms and the gold-standard Gibbs methods are shown on top of the corresponding index-wise marginal variances. Columns: Different measurements.

covered if $\log p_{\mathbf{x}|\mathbf{Y}=\mathbf{y}}(\mathbf{x}) \geq l_{\lceil \alpha N_{\text{samples}} \rceil}(\mathbf{y})$ and define the coverage of a method as

$$\frac{1}{N_{\text{test}}} \sum_{k=1}^{N_{\text{test}}} \chi_{\mathbb{R} \geq l_{\lceil \alpha N_{\text{samples}} \rceil}(\mathbf{y}_k^{\text{test}})}(\log p_{\mathbf{x}|\mathbf{Y}=\mathbf{y}_k^{\text{test}}}(\mathbf{x}_k^{\text{test}})). \quad (55)$$

The coverage of a sampling method that really draws samples from the posterior will be α up to Monte Carlo error. A coverage result that is significantly less than α indicates that the samples obtained by the method concentrate too heavily around the mode; a coverage result that is greater than α indicates that the samples are too spread out. The coverage results for $\alpha = 0.9$ are presented in table IV. The Gibbs row again validates the implementation; for all forward operators, they achieve coverages that are very close to 0.9. In contrast, the coverage values obtained by the DPS algorithms are generally much smaller than 0.9. For C-DPS and DiffPIR, the reported coverage values are almost always 0 except for BL(0.1, 1) and St(1) jumps, where the coverages are usually (close to) 1 for C-DPS and inconsistent for DiffPIR. For almost all jump distributions and forward operators, DPnP reports coverage values that are closest to but typically smaller than 0.9.¹⁰

VI. CONCLUSION

We introduced a framework for the objective benchmarking of diffusion posterior sampling algorithms. The framework relies on the construction of signals with known distribution, the simulation of the measurement process, and the subsequent generation of samples from the posterior distribution that arises through the combination of the known prior and the known likelihood. Gold-standard samples from that distribution are then acquired by efficient Gibbs methods and these samples can be compared to those obtained by the diffusion posterior sampling algorithms. In addition, the Gibbs methods can serve as oracle MMSE denoisers in the denoising problems that are encountered in each iteration of the reverse SDE. Consequently, the framework also enables the quantification of the additional errors that are incurred through any suboptimal learned components.

We provided numerical results for three common posterior sampling algorithms applied to four common inverse problems and invite other researcher to benchmark their algorithms on our open implementation that is deliberately designed such that novel DPS algorithms can be benchmarked in a plug-and-play manner. A common theme among all tested algorithms is that the samples they produce are not calibrated, which demonstrates that research for algorithms that perform better in this respect is still crucial.

REFERENCES

[1] R. Rombach, A. Blattmann, D. Lorenz, P. Esser, and B. Ommer, “High-resolution image synthesis with latent diffusion models,” in *2022 IEEE/CVF Conference on Computer Vision and Pattern Recognition (CVPR)*, IEEE, Jun. 2022, pp. 10 674–10 685. DOI: [10.1109/cvpr52688.2022.01042](https://doi.org/10.1109/cvpr52688.2022.01042).

¹⁰Note that a coverage of 1 can be considered the worst case even at a target of 0.9. For instance, it is achieved by setting all samples to a constant vector with extremely large (i.e. “unlikely”) entries.

[2] R. Po, W. Yifan, V. Golyanik, *et al.*, “State of the art on diffusion models for visual computing,” *Computer Graphics Forum*, vol. 43, no. 2, Apr. 2024, ISSN: 1467-8659. DOI: [10.1111/cgf.15063](https://doi.org/10.1111/cgf.15063).

[3] H. Huang, M. Chen, and X. Qiao, “Generative learning for financial time series with irregular and scale-invariant patterns,” in *The Twelfth International Conference on Learning Representations*, 2024.

[4] K. Rasul, C. Seward, I. Schuster, and R. Vollgraf, “Autoregressive denoising diffusion models for multivariate probabilistic time series forecasting,” in *International conference on Machine Learning*, PMLR, 2021, pp. 8857–8868.

[5] J. L. Watson, D. Juergens, N. R. Bennett, *et al.*, “De novo design of protein structure and function with RFdiffusion,” *Nature*, vol. 620, no. 7976, pp. 1089–1100, Jul. 2023, ISSN: 1476-4687. DOI: [10.1038/s41586-023-06415-8](https://doi.org/10.1038/s41586-023-06415-8).

[6] A. Alakhdar, B. Poczos, and N. Washburn, “Diffusion models in de novo drug design,” *Journal of Chemical Information and Modeling*, vol. 64, no. 19, pp. 7238–7256, Sep. 2024, ISSN: 1549-960X. DOI: [10.1021/acs.jcim.4c01107](https://doi.org/10.1021/acs.jcim.4c01107).

[7] X. L. Li, J. Thickstun, I. Gulrajani, P. Liang, and T. Hashimoto, “Diffusion-LM improves controllable text generation,” in *Advances in Neural Information Processing Systems*, A. H. Oh, A. Agarwal, D. Belgrave, and K. Cho, Eds., 2022.

[8] S. Gong, M. Li, J. Feng, Z. Wu, and L. Kong, “Diffuseq: Sequence to sequence text generation with diffusion models,” in *The Eleventh International Conference on Learning Representations*, 2023.

[9] M. Ren, M. Delbracio, H. Talebi, G. Gerig, and P. Milanfar, “Multiscale structure guided diffusion for image deblurring,” in *2023 IEEE/CVF International Conference on Computer Vision (ICCV)*, Los Alamitos, CA, USA: IEEE Computer Society, Oct. 2023, pp. 10 687–10 699. DOI: [10.1109/ICCV51070.2023.00984](https://doi.org/10.1109/ICCV51070.2023.00984).

[10] D. Xue, W. Dai, Z. Zheng, X. Peng, J. Zou, and H. Xiong, “Fourier phase retrieval with diffusion priors guided by failure detection,” in *2025 IEEE International Symposium on Circuits and Systems (ISCAS)*, 2025, pp. 1–5. DOI: [10.1109/ISCAS56072.2025.11042933](https://doi.org/10.1109/ISCAS56072.2025.11042933).

[11] H. Chung and J. C. Ye, “Score-based diffusion models for accelerated MRI,” *Medical Image Analysis*, vol. 80, p. 102 479, 2022, ISSN: 1361-8415. DOI: <https://doi.org/10.1016/j.media.2022.102479>.

[12] J. Liu, R. Anirudh, J. J. Thiagarajan, *et al.*, “DOLCE: A model-based probabilistic diffusion framework for limited-angle CT reconstruction,” in *2023 IEEE/CVF International Conference on Computer Vision (ICCV)*, 2023, pp. 10 464–10 474. DOI: [10.1109/ICCV51070.2023.00963](https://doi.org/10.1109/ICCV51070.2023.00963).

[13] O. Özdenizci and R. Legenstein, “Restoring vision in adverse weather conditions with patch-based denoising diffusion models,” *IEEE Transactions on Pattern Analysis and Machine Intelligence*, pp. 1–12, 2023. DOI: [10.1109/TPAMI.2023.3238179](https://doi.org/10.1109/TPAMI.2023.3238179).

| | | Gauss(0, 0.25) | | Laplace(1) | | BL(0.1, 1) | | St(1) | | St(2) | | St(3) | |
|---------------|---------|----------------|--------|------------|--------|------------|--------|---------|--------|---------|--------|---------|--------|
| | | Learned | Oracle | Learned | Oracle | Learned | Oracle | Learned | Oracle | Learned | Oracle | Learned | Oracle |
| Denoising | Gibbs | — | 0.90 | — | 0.91 | — | 0.91 | — | 0.89 | — | 0.91 | — | 0.89 |
| | C-DPS | 0.00 | 0.00 | 0.00 | 0.00 | 1.00 | 1.00 | 1.00 | 1.00 | 0.00 | 0.00 | 0.00 | 0.00 |
| | DiffPIR | 0.00 | 0.00 | 0.00 | 0.00 | 1.00 | 1.00 | 0.28 | 0.02 | 0.00 | 0.00 | 0.00 | 0.00 |
| | DPnP | 0.58 | 0.67 | 0.11 | 0.11 | 1.00 | 0.41 | 0.53 | 0.08 | 0.09 | 0.09 | 0.09 | 0.10 |
| Deconvolution | Gibbs | — | 0.89 | — | 0.90 | — | 0.90 | — | 0.91 | — | 0.91 | — | 0.91 |
| | C-DPS | 0.00 | 0.00 | 0.01 | 0.00 | 1.00 | 1.00 | 1.00 | 0.83 | 0.01 | 0.00 | 0.00 | 0.00 |
| | DiffPIR | 0.00 | 0.00 | 0.00 | 0.00 | 1.00 | 1.00 | 0.97 | 0.92 | 0.00 | 0.00 | 0.00 | 0.00 |
| | DPnP | 0.12 | 0.12 | 0.06 | 0.07 | 1.00 | 0.31 | 0.50 | 0.06 | 0.06 | 0.06 | 0.07 | 0.06 |
| Imputation | Gibbs | — | 0.89 | — | 0.90 | — | 0.86 | — | 0.91 | — | 0.91 | — | 0.91 |
| | C-DPS | 0.00 | 0.00 | 0.00 | 0.00 | 1.00 | 1.00 | 0.94 | 0.78 | 0.15 | 0.15 | 0.00 | 0.00 |
| | DiffPIR | 0.00 | 0.00 | 0.00 | 0.00 | 1.00 | 1.00 | 0.72 | 0.32 | 0.00 | 0.00 | 0.00 | 0.00 |
| | DPnP | 0.28 | 0.31 | 0.09 | 0.08 | 1.00 | 0.41 | 0.56 | 0.07 | 0.14 | 0.13 | 0.12 | 0.13 |
| Fourier | Gibbs | — | 0.91 | — | 0.90 | — | 0.90 | — | 0.91 | — | 0.92 | — | 0.91 |
| | C-DPS | 0.00 | 0.00 | 0.00 | 0.00 | 1.00 | 1.00 | 0.96 | 0.74 | 0.01 | 0.01 | 0.00 | 0.00 |
| | DiffPIR | 0.00 | 0.00 | 0.00 | 0.00 | 1.00 | 1.00 | 0.92 | 0.65 | 0.00 | 0.01 | 0.00 | 0.00 |
| | DPnP | 0.19 | 0.19 | 0.08 | 0.06 | 1.00 | 0.32 | 0.50 | 0.06 | 0.07 | 0.07 | 0.07 | 0.06 |

TABLE IV: Posterior coverage of various estimation methods at $\alpha = 0.9$.

- [14] L. Bogensperger, D. Narnhofer, A. Allam, K. Schindler, and M. Krauthammer, “A variational perspective on generative protein fitness optimization,” in *Forty-second International Conference on Machine Learning*, 2025.
- [15] J.-M. Lemerrier, J. Richter, S. Welker, E. Moliner, V. Välimäki, and T. Gerkmann, “Diffusion models for audio restoration: A review,” *IEEE Signal Processing Magazine*, vol. 41, no. 6, pp. 72–84, 2024. DOI: [10.1109/MSP.2024.3445871](#).
- [16] Z. Wang and C. Ventre, “A financial time series denoiser based on diffusion models,” in *Proceedings of the 5th ACM International Conference on AI in Finance*, ser. ICAIF ’24, Brooklyn, NY, USA: Association for Computing Machinery, 2024, pp. 72–80, ISBN: 9798400710810. DOI: [10.1145/3677052.3698649](#).
- [17] N. Yismaw, U. S. Kamilov, and M. S. Asif, “Covariance-corrected diffusion models for solving inverse problems,” in *2025 IEEE Statistical Signal Processing Workshop (SSP)*, 2025, pp. 26–30. DOI: [10.1109/SSP64130.2025.11073300](#).
- [18] J. Erbach, D. Narnhofer, A. Dombos, B. Schiele, J. E. Lenssen, and K. Schindler, “Solving inverse problems with FLAIR,” 2025, arXiv. DOI: [10.48550/arXiv.2506.02680](#).
- [19] Z. Wang, A. Bovik, H. Sheikh, and E. Simoncelli, “Image quality assessment: From error visibility to structural similarity,” *IEEE Transactions on Image Processing*, vol. 13, no. 4, pp. 600–612, 2004. DOI: [10.1109/TIP.2003.819861](#).
- [20] M. Heusel, H. Ramsauer, T. Unterthiner, B. Nessler, and S. Hochreiter, “GANs trained by a two time-scale update rule converge to a local Nash equilibrium,” in *Proceedings of the 31st International Conference on Neural Information Processing Systems*, ser. NIPS’17, Long Beach, California, USA: Curran Associates Inc., 2017, pp. 6629–6640, ISBN: 9781510860964.
- [21] R. Zhang, P. Isola, A. A. Efros, E. Shechtman, and O. Wang, “The unreasonable effectiveness of deep features as a perceptual metric,” in *2018 IEEE/CVF Conference on Computer Vision and Pattern Recognition*, 2018, pp. 586–595. DOI: [10.1109/CVPR.2018.00068](#).
- [22] E. Pierret and B. Galerne, “Diffusion models for Gaussian distributions: Exact solutions and Wasserstein errors,” in *Forty-second International Conference on Machine Learning*, 2025.
- [23] B. Boys, M. Girolami, J. Pidstrigach, S. Reich, A. Mosca, and O. D. Akyildiz, “Tweedie moment projected diffusions for inverse problems,” *Transactions on Machine Learning Research*, 2024, Featured Certification, ISSN: 2835-8856.
- [24] E. S. Crafts and U. Villa, “Benchmarking diffusion annealing-based Bayesian inverse problem solvers,” *IEEE Open Journal of Signal Processing*, vol. 6, pp. 975–991, 2025. DOI: [10.1109/OJSP.2025.3597867](#).
- [25] R. C. Blattberg and N. J. Gonedes, “A comparison of the stable and student distributions as statistical models for stock prices,” *The Journal of Business*, vol. 47, no. 2, pp. 244–280, 1974, ISSN: 00219398, 15375374.
- [26] R. Cont, “Empirical properties of asset returns: Stylized facts and statistical issues,” *Quantitative Finance*, vol. 1, no. 2, pp. 223–236, 2001. DOI: [10.1080/713665670](#).
- [27] M. J. Wainwright and E. Simoncelli, “Scale mixtures of Gaussians and the statistics of natural images,” in *Advances in Neural Information Processing Systems*, S.olla, T. Leen, and K. Müller, Eds., vol. 12, MIT Press, 1999.
- [28] P. Bohra, P. del Aguila Pla, J.-F. Giovannelli, and M. Unser, “A statistical framework to investigate the optimality of signal-reconstruction methods,” *IEEE Transactions on Signal Processing*, vol. 71, pp. 2043–2055, 2023. DOI: [10.1109/TSP.2023.3282062](#).
- [29] X. Xu and Y. Chi, “Provably robust score-based diffusion posterior sampling for plug-and-play image reconstruction,” in *The Thirty-eighth Annual Conference on Neural Information Processing Systems*, 2024.

- [30] O. Scherzer, M. Grasmair, H. Grossauer, M. Haltmeier, and F. Lenzen, *Variational Methods in Imaging* (Applied mathematical sciences), en, 2009th ed. New York, NY: Springer, Oct. 2008.
- [31] R. Bassett and J. Deride, “Maximum a posteriori estimators as a limit of Bayes estimators,” *Mathematical Programming*, vol. 174, no. 1–2, pp. 129–144, Jan. 2018, ISSN: 1436-4646. DOI: [10.1007/s10107-018-1241-0](https://doi.org/10.1007/s10107-018-1241-0).
- [32] C. Clason, T. Helin, R. Kretschmann, and P. Piiroinen, “Generalized modes in bayesian inverse problems,” *SIAM/ASA Journal on Uncertainty Quantification*, vol. 7, no. 2, pp. 652–684, 2019. DOI: [10.1137/18M1191804](https://doi.org/10.1137/18M1191804).
- [33] Y. Song, J. Sohl-Dickstein, D. P. Kingma, A. Kumar, S. Ermon, and B. Poole, “Score-based generative modeling through stochastic differential equations,” in *International Conference on Learning Representations*, 2021.
- [34] Y. Song and S. Ermon, “Generative modeling by estimating gradients of the data distribution,” in *Advances in Neural Information Processing Systems*, 2019, pp. 11 895–11 907.
- [35] J. Ho, A. Jain, and P. Abbeel, “Denoising diffusion probabilistic models,” in *Proceedings of the 34th International Conference on Neural Information Processing Systems*, ser. NIPS ’20, Vancouver, BC, Canada: Curran Associates Inc., 2020, ISBN: 9781713829546.
- [36] A. Klenke, *Probability Theory: A Comprehensive Course*. Springer International Publishing, 2020, ISBN: 9783030564025. DOI: [10.1007/978-3-030-56402-5](https://doi.org/10.1007/978-3-030-56402-5).
- [37] B. D. Anderson, “Reverse-time diffusion equation models,” *Stochastic Processes and their Applications*, vol. 12, no. 3, pp. 313–326, 1982, ISSN: 0304-4149. DOI: [10.1016/0304-4149\(82\)90051-5](https://doi.org/10.1016/0304-4149(82)90051-5).
- [38] H. Chung, J. Kim, M. T. McCann, M. L. Klasky, and J. C. Ye, “Diffusion posterior sampling for general noisy inverse problems,” in *The Eleventh International Conference on Learning Representations*, 2023.
- [39] G. Daras, A. G. Dimakis, and C. Daskalakis, “Consistent diffusion meets Tweedie: Training exact ambient diffusion models with noisy data,” in *Proceedings of the 41st International Conference on Machine Learning*, ser. ICML’24, Vienna, Austria: JMLR.org, 2024.
- [40] C. W. Gardiner, *Handbook of stochastic methods: For physics, chemistry and the natural sciences*, en. Berlin, Germany: Springer, 1990.
- [41] P. Vincent, “A connection between score matching and denoising autoencoders,” *Neural Computation*, vol. 23, no. 7, pp. 1661–1674, 2011. DOI: [10.1162/NECO_a_00142](https://doi.org/10.1162/NECO_a_00142).
- [42] D. J. Higham, “An algorithmic introduction to numerical simulation of stochastic differential equations,” *SIAM Review*, vol. 43, no. 3, pp. 525–546, 2001. DOI: [10.1137/S0036144500378302](https://doi.org/10.1137/S0036144500378302).
- [43] J. Sohl-Dickstein, E. Weiss, N. Maheswaranathan, and S. Ganguli, “Deep unsupervised learning using nonequilibrium thermodynamics,” in *Proceedings of the 32nd International Conference on Machine Learning*, F. Bach and D. Blei, Eds., ser. Proceedings of Machine Learning Research, vol. 37, Lille, France: PMLR, Jul. 2015, pp. 2256–2265.
- [44] C. Saharia, J. Ho, W. Chan, T. Salimans, D. J. Fleet, and M. Norouzi, “Image super-resolution via iterative refinement,” *IEEE Transactions on Pattern Analysis and Machine Intelligence*, vol. 45, no. 4, pp. 4713–4726, 2023. DOI: [10.1109/TPAMI.2022.3204461](https://doi.org/10.1109/TPAMI.2022.3204461).
- [45] A. Jalal, M. Arvinte, G. Daras, E. Price, A. G. Dimakis, and J. Tamir, “Robust compressed sensing MRI with deep generative priors,” in *Advances in Neural Information Processing Systems*, M. Ranzato, A. Beygelzimer, Y. Dauphin, P. Liang, and J. W. Vaughan, Eds., vol. 34, Curran Associates, Inc., 2021, pp. 14 938–14 954.
- [46] Y. Zhu, K. Zhang, J. Liang, *et al.*, “Denoising diffusion models for plug-and-play image restoration,” in *IEEE Conference on Computer Vision and Pattern Recognition Workshops (NTIRE)*, 2023.
- [47] G. Daras, H. Chung, C.-H. Lai, *et al.*, *A survey on diffusion models for inverse problems*, arXiv, 2024. DOI: [10.48550/arXiv.2410.00083](https://doi.org/10.48550/arXiv.2410.00083).
- [48] X. Gao, H. M. Nguyen, and L. Zhu, “Wasserstein convergence guarantees for a general class of score-based generative models,” *Journal of Machine Learning Research*, vol. 26, no. 43, pp. 1–54, 2025.
- [49] S. Strasman, A. Ocello, C. Boyer, S. L. Corff, and V. Lemaire, “An analysis of the noise schedule for score-based generative models,” *Transactions on Machine Learning Research*, 2025, ISSN: 2835-8856.
- [50] S. Hurault, M. Terris, T. Moreau, and G. Peyré, *From score matching to diffusion: A fine-grained error analysis in the Gaussian setting*, arXiv, 2025. DOI: [10.48550/arXiv.2503.11615](https://doi.org/10.48550/arXiv.2503.11615).
- [51] E. Pierret and B. Galerne, *Exact evaluation of the accuracy of diffusion models for inverse problems with Gaussian data distributions*, arXiv, 2025. DOI: [10.48550/arXiv.2507.07008](https://doi.org/10.48550/arXiv.2507.07008).
- [52] D. Y. W. Thong, C. K. Mbakam, and M. Pereyra, *Do Bayesian imaging methods report trustworthy probabilities?* arXiv, 2024. DOI: [10.48550/arXiv.2405.08179](https://doi.org/10.48550/arXiv.2405.08179).
- [53] M. Unser and P. D. Tafti, *An Introduction to Sparse Stochastic Processes*. Cambridge University Press, 2014.
- [54] K.-I. Sato, *Lévy processes and infinitely divisible distributions* (Cambridge studies in advanced mathematics), ja. Cambridge, England: Cambridge University Press, Nov. 1999.
- [55] W. Schoutens, *Lévy processes in finance* (Wiley Series in Probability and Statistics), en. Chichester, England: John Wiley & Sons, Mar. 2003.
- [56] M. Kuric, M. Zach, A. Habring, M. Unser, and T. Pock, *The Gaussian latent machine: Efficient prior and posterior sampling for inverse problems*, arXiv, 2025. DOI: [10.48550/arXiv.2505.12836](https://doi.org/10.48550/arXiv.2505.12836).
- [57] A. Gelman, J. B. Carlin, H. S. Stern, D. B. Dunson, A. Vehtari, and D. B. Rubin, *Bayesian Data Analysis*. Chapman and Hall/CRC, Nov. 2013, ISBN: 9780429113079. DOI: [10.1201/b16018](https://doi.org/10.1201/b16018).
- [58] G. Casella and E. I. George, “Explaining the Gibbs sampler,” *The American Statistician*, vol. 46, no. 3,

- pp. 167–174, Aug. 1992, ISSN: 1537-2731. DOI: [10.1080/00031305.1992.10475878](https://doi.org/10.1080/00031305.1992.10475878).
- [59] D. A. van Dyk and T. Park, “Partially collapsed gibbs samplers,” *Journal of the American Statistical Association*, vol. 103, no. 482, pp. 790–796, 2008. DOI: [10.1198/016214508000000409](https://doi.org/10.1198/016214508000000409).
- [60] L. Devroye, “Random variate generation for the generalized inverse Gaussian distribution,” *Statistics and Computing*, vol. 24, no. 2, pp. 239–246, Dec. 2012, ISSN: 1573-1375. DOI: [10.1007/s11222-012-9367-z](https://doi.org/10.1007/s11222-012-9367-z).
- [61] A. Paszke, S. Gross, S. Chintala, *et al.*, “Automatic differentiation in pytorch,” in *NIPS-W*, 2017.
- [62] H. T. V. Le, M. Foare, A. Repetti, and N. Pustelnik, “Embedding Blake–Zisserman regularization in unfolded proximal neural networks for enhanced edge detection,” *IEEE Signal Processing Letters*, vol. 32, pp. 1271–1275, 2025. DOI: [10.1109/LSP.2025.3547671](https://doi.org/10.1109/LSP.2025.3547671).
- [63] S. Rissanen, M. Heinonen, and A. Solin, “Free hunch: Denoiser covariance estimation for diffusion models without extra costs,” in *The Thirteenth International Conference on Learning Representations*, 2025.

APPENDIX

A. Connection between the Reverse SDE and DDPM Sampling

The DDPM model has been introduced in [43] as a discrete-time Markov chain of length T with Gaussian transitions

$$p_{\mathbf{X}_t|\mathbf{X}_{t-1}=\mathbf{x}_{t-1}} = \text{Gauss}(\sqrt{1-\beta_t}\mathbf{x}_{t-1}, \beta_t\mathbf{I}) \quad (56)$$

such that the transitions from \mathbf{X}_0 to \mathbf{X}_t are also tractable as

$$\mathbf{X}_t = \sqrt{\alpha_t}\mathbf{X}_0 + \sqrt{1-\alpha_t}\mathbf{Z}_t \quad (57)$$

where $\alpha_t = 1 - \beta_t$, $\bar{\alpha}_t = \prod_{s=0}^t \alpha_s$ and $\mathbf{Z}_t \sim \text{Gauss}(\mathbf{0}, \mathbf{I})$. By definition,

$$\mathbf{X}_t = \sqrt{1-\beta_t}\mathbf{X}_{t-1} + \sqrt{\beta_t}\mathbf{Z}_{t-1}, \quad (58)$$

which, by a straightforward application of Tweedie’s formula

$$\mathbb{E}[\mathbf{X}_{t-1}|\mathbf{X}_t] = \frac{1}{\sqrt{\alpha_t}} (\mathbf{X}_t + (1-\alpha_t)\nabla \log p_{\mathbf{X}_t}(\mathbf{X}_t)) \quad (59)$$

leads to the backward transitions

$$\mathbf{X}_{t-1} = \frac{1}{\sqrt{1-\beta_t}} (\mathbf{X}_t + \beta_t \nabla \log p_{\mathbf{X}_t}(\mathbf{X}_t)) + \sqrt{\beta_t}\mathbf{Z}_t. \quad (60)$$

The Euler–Maruyama discretization of the backward Ornstein–Uhlenbeck SDE given in (20) and repeated here as

$$\mathbf{X}_{t-1} = (1 + \frac{\beta_t}{2})\mathbf{X}_t + \beta_t \nabla \log p_{\mathbf{X}_t}(\mathbf{X}_t) + \sqrt{\beta_t}\mathbf{Z}_t \quad (61)$$

can be related to the DDPM updates via Taylor expansions since

$$\frac{1}{\sqrt{1-\beta_t}} = 1 + \frac{\beta_t}{2} + O(\beta_t^2) \quad (62)$$

and

$$\frac{\beta_t}{\sqrt{1-\beta_t}} = \beta_t + O(\beta_t^2). \quad (63)$$

B. Covariance in DPS

C-DPS [38] uses the approximation of the likelihood

$$p_{\mathbf{Y}|\mathbf{X}_t=\mathbf{x}}(\mathbf{y}) \approx p_{\mathbf{Y}|\mathbf{X}_0=\mathbb{E}[\mathbf{X}_0|\mathbf{X}_t=\mathbf{x}]}(\mathbf{y}). \quad (64)$$

When the noise in the inverse problem is Gaussian, the computation of $\nabla \log(\mathbf{x} \mapsto p_{\mathbf{Y}|\mathbf{X}_0=\mathbb{E}[\mathbf{X}_0|\mathbf{X}_t=\mathbf{x}]}(\mathbf{y}))$ necessitates the computation of

$$\nabla (\mathbf{x} \mapsto \frac{1}{2} \|\mathbf{A}\mathbb{E}[\mathbf{X}_0 | \mathbf{X}_t = \mathbf{x}] - \mathbf{y}\|^2), \quad (65)$$

which is

$$\mathbf{J}(\mathbf{x} \mapsto \mathbb{E}[\mathbf{X}_0 | \mathbf{X}_t = \mathbf{x}]) (\cdot) \mathbf{A}^T (\mathbf{A}\mathbb{E}[\mathbf{X}_0 | \mathbf{X}_t = \cdot] - \mathbf{y}) \quad (66)$$

after an application of the chain rule. The Jacobian $\mathbf{J}(\mathbf{x} \mapsto \mathbb{E}[\mathbf{X}_0 | \mathbf{X}_t = \mathbf{x}])$ is typically computed with automatic differentiation when $(\mathbf{x}, t) \mapsto \mathbb{E}[\mathbf{X}_0 | \mathbf{X}_t = \mathbf{x}]$ is approximated with a neural network. In our framework, we use the connection with the covariance matrix $\text{Cov}[\mathbf{X}_0 | \mathbf{X}_t = \cdot]$. Indeed, as also shown in, *e.g.*, [63], if \mathbf{X}_0 and \mathbf{X}_t verify (57), then

$$\frac{1}{1-\bar{\alpha}_t} \text{Cov}[\mathbf{X}_0 | \mathbf{X}_t = \mathbf{x}] = \frac{1}{\bar{\alpha}_t} (\mathbf{I} + (1-\bar{\alpha}_t)^2 \nabla^2 \log p_{\mathbf{X}_t}(\mathbf{x})). \quad (67)$$

This identity combined with the derivative of (19) yields

$$\mathbf{J}(\mathbf{x} \mapsto \mathbb{E}[\mathbf{X}_0 | \mathbf{X}_t = \mathbf{x}]) (\mathbf{x}_t) = \frac{\sqrt{\bar{\alpha}_t}}{1-\bar{\alpha}_t} \text{Cov}[\mathbf{X}_0 | \mathbf{X}_t = \mathbf{x}_t]. \quad (68)$$

C. A Protocol to Determine the Burn-In Period and the Number of Samples

As discussed in section IV-B, the burn-in period and the number of samples of the Gibbs samplers needs to be chosen appropriately to ensure an acceptable runtime of the benchmark when they serve as the gold-standard samplers of the denoising problems that are encountered in the DPS algorithms. We determine the burn-in period and the number of samples through the following protocol that is run in an off-line stage prior to running the benchmark. We take one datum $\mathbf{x}_t = \mathbf{x}_0 + \sigma_n \mathbf{n}$ where \mathbf{x}_0 is constructed via (28) where p_U is a $\text{St}(1)$ distribution and \mathbf{n} is some unknown but fixed vector of standard Gaussian noise. We then launch $C = 1000$ parallel Gibbs chains on the corresponding denoising problem and run those chains for $N_{\text{sufficient}}$ iterations, where $N_{\text{sufficient}}$ is a sufficiently large natural number that guarantees that the chains are stationary for at least N_{avg} (which is also relatively large) iterations and that, consequently, we can compute precise estimates of various statistics of the posterior distribution from the iterates from the last N_{avg} iterations across all C chains.

To determine the burn-in period, we then proceed to calculate a statistic that we can monitor throughout the iterations and that we can compare against the reference statistic. Specifically, denoting with \mathbf{X} the random variable of the Gibbs sampler, we compute the empirical distribution of the jumps at index 32, that is, $\mathbf{X}_{33} - \mathbf{X}_{32}$. The distribution of differences that is obtained by taking the last N_{avg} iterations across all C chains is considered the reference distribution. Then, we compute the Wasserstein-1 distance of that distribution to the one obtained by taking the average across N_{avg} iterations and all C in a sliding-window starting from the first Gibbs iterations. This allows

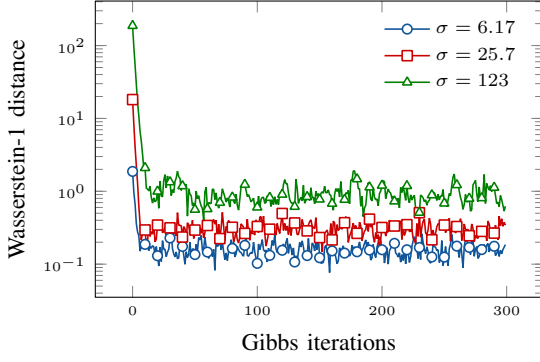


Fig. 5: Wasserstein-1 distance of the intermediate distribution of $\mathbf{X}_{33} - \mathbf{X}_{32}$ during the iterations to that of the final sample.

us to gauge the burn-in period through a visual inspection of the Wasserstein-1 distance through the Gibbs iterations. In particular, we expect the Wasserstein-1 distance to be large for a number of initial samples where the Gibbs sampler is not stationary and then to oscillate around a small but nonzero value. The value will be nonzero due to the finite sample size. The Wasserstein-1 distance between the reference distribution and the one obtained through the Gibbs iterations is shown in [fig. 5](#). We observe that the empirical distribution of jumps converges rapidly to the reference one. The Wasserstein-1 distance reaches the noise level after a single-digit number of iterations, which is in line with the analysis provided in [\[56\]](#). Based on these findings, we chose the burn-in period as $B = 100$ iterations for all our experiments, which is more than sufficient to reach stationarity and has acceptable runtime.

To determine the number of samples that are needed for a sufficiently accurate computation of various statistics that any DPS algorithm may utilize in their update steps, we compute a precise estimation of the MMSE estimate of the denoising problem by averaging the last N_{avg} iterations across all C chains. Then, we pick an arbitrary chain and grow a window from iteration $(N_{\text{avg}} - 1)$ to the left, average the samples in that window, and compute the MSE from the MMSE estimates obtained in the one-chain window to the precise estimate obtained by averaging the C chains and the last N_{avg} iterations. We pick a tolerance of 1×10^{-2} and monitor at which window length the MSE falls below that tolerance. The results in [fig. 6](#) show that this tolerance is consistently reached when the averaging window is 300 samples long, which motivates our choice of using $S = 300$ samples for all our experiments.

D. Algorithm Parameter Identification

The grid for the model-based methods was a loglinear grid $\Lambda = \{\lambda_1, \lambda_2, \dots, \lambda_{N_{\text{mb}}}\}$ where

$$\lambda_i = 10^{a+(i-1)\frac{(b-a)}{N_{\text{mb}}-1}} \quad (69)$$

with $a = -5$ and $b = 5$. Since the model-based methods are very fast, we can use the relatively high $N_{\text{mb}} = 1000$. The MSE over the validation data set of the ℓ_2 and ℓ_1 estimators are shown in [fig. 7](#).

For the DPS algorithms we define a modest number of $N_{\text{dps}} = 40$ grid-points and found the extreme points of the grid

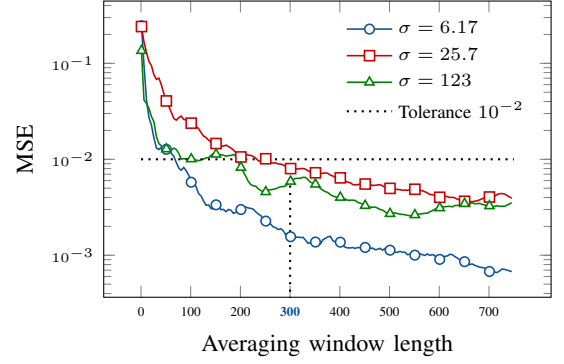


Fig. 6: MSE gap to the long-run MMSE normalized by σ^2 .

(i.e. values of the parameters that clearly lead to worse results) by hand. For C-DPS and DiffPIR, we fix the diffusion schedule to standard choices ($\beta_0 = 1 \times 10^{-4}$, $\beta_T = 0.02$). In addition to the diffusion schedule, C-DPS has one tunable parameter ζ that we tune on 40 loglinear grid points ($i = 1, \dots, N_{\text{dps}}$)

$$10^{a+(i-1)\frac{(b-a)}{N_{\text{dps}}-1}}, \quad (70)$$

where $a = -3$ and $b = 1$. DiffPIR has two tunable parameters ζ and ρ , although ζ is typically considered not so critical. Thus, we split the 40 grid points into a two-dimensional grid $\Theta^{\text{DiffPIR}} = \{0.3, 0.7\} \times \Theta^\rho$, i.e., 2 points for ζ and 20 points for ρ given by $\Theta^\rho = \{\Theta_1^\rho, \dots, \Theta_{N_{\text{dps}}/2}^\rho\}$ where

$$\Theta_1^\rho = 10^{a+(i-1)\frac{(b-a)}{(N_{\text{dps}}/2)-1}} \quad (71)$$

with $a = -4$ and $b = 1$. The DPnP algorithm only has the schedule $\{\eta_t\}_{t=1}^T$ to tune. In this case, since DPnP is asymptotically correct, the schedule is a practical vehicle that enables to trade off between speed and accuracy. Therefore, we use a schedule that is similar to the one that was proposed in the original publication [\[29\]](#): We fix a small $\eta_{\text{final}} = 0.15$, and linearly decrease eta from some η_{initial} to η_{final} after $K/5$ initial iterations with η_{initial} :

$$\eta_i = \begin{cases} \eta_{\text{initial}} & \text{if } i = 1, \dots, K/5 \\ \frac{\eta_{\text{final}}}{\eta_{\text{initial}}} \frac{i-K/5}{K-K/5} \eta_{\text{initial}} & \text{if } i = K/5 + 1, \dots, K \end{cases} \quad (72)$$

We treat η_{initial} as a tunable parameter and search over $\Theta^{\text{DPnP}} = \{\eta_1, \eta_2, \dots, \eta_{40}\}$ where for $i = 1, \dots, 40$,

$$\eta_i = 10^{a+(i-1)\frac{(b-a)}{40-1}} \quad (73)$$

with $a = -1$ and $b = 4$. Like in the original publication, we use the comparatively small $K = 40$.

The MSE over the validation data set of C-DPS, DiffPIR, and DPnP for the various parameter choices is shown in [fig. 7](#). Since the ζ parameter of DiffPIR is considered not so critical, we only show the values of the MSE for various choices of ρ where ζ is set to the value of the optimal (ζ, ρ) pair.

E. Additional Results

[Figure 4](#) in the main body of the manuscript showed the results for deconvolution using the oracle denoiser. [Figure 10](#) shows the results for deconvolution using the learned denoiser.

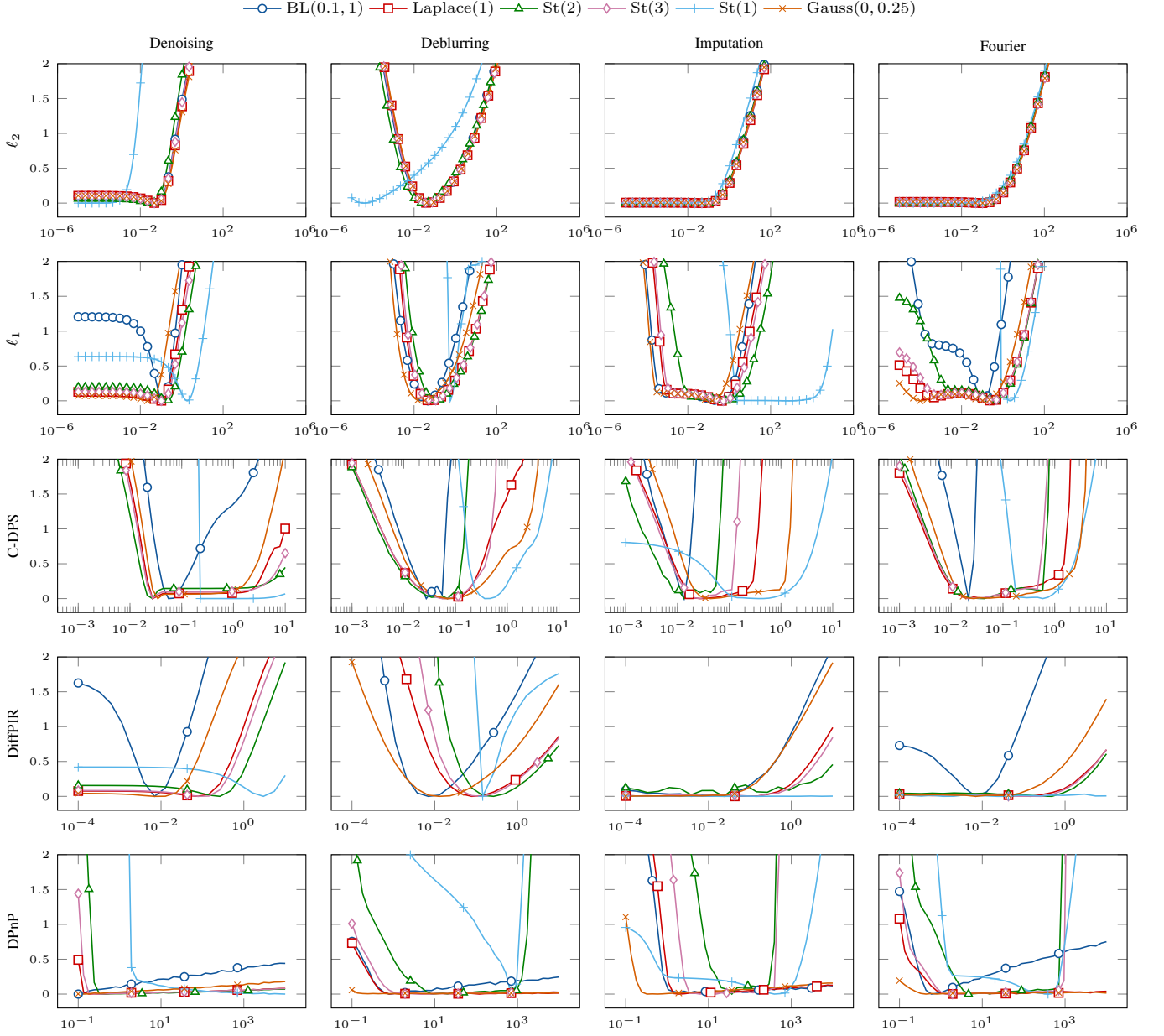


Fig. 7: Grid search diagnostics (logarithm of the MSE over the validation data set) for the DPS algorithms. Rows: ℓ_2 ; ℓ_1 ; C-DPS; DiffPIR; DPnP. Columns: Denoising; deconvolution; imputation; reconstruction from partial Fourier measurements. For better visualization, each curve has had its minimum subtracted. To avoid clutter, marks are placed only at every 10th grid point.

Figures 11 to 16 show the results for denoising and imputation using the oracle and learned denoisers.

F. Latent Distributions and Notation

Some of the distributions that we rely on in this work have multiple competing parametrizations and we provide a summary of our definitions in table V to avoid any ambiguities. Table VI lists the latent maps and conditional latent distributions that are needed for the GLM for the distributions in this work.

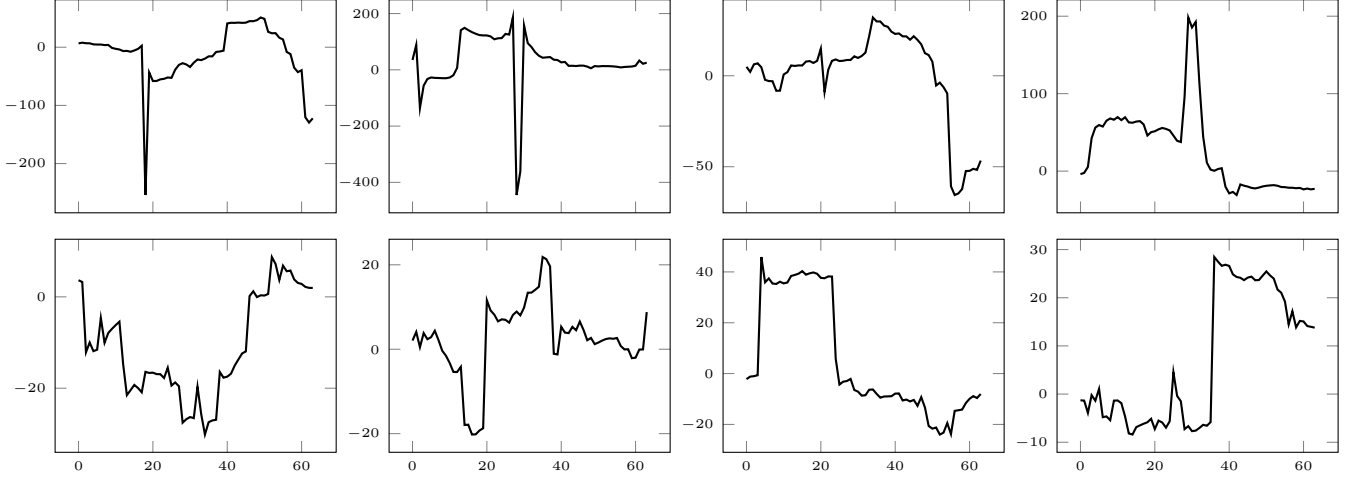


Fig. 8: Unconditional samples obtained by DDPM with the learned denoiser (top) and the oracle denoiser (bottom). Columns: Different initializations and random states.

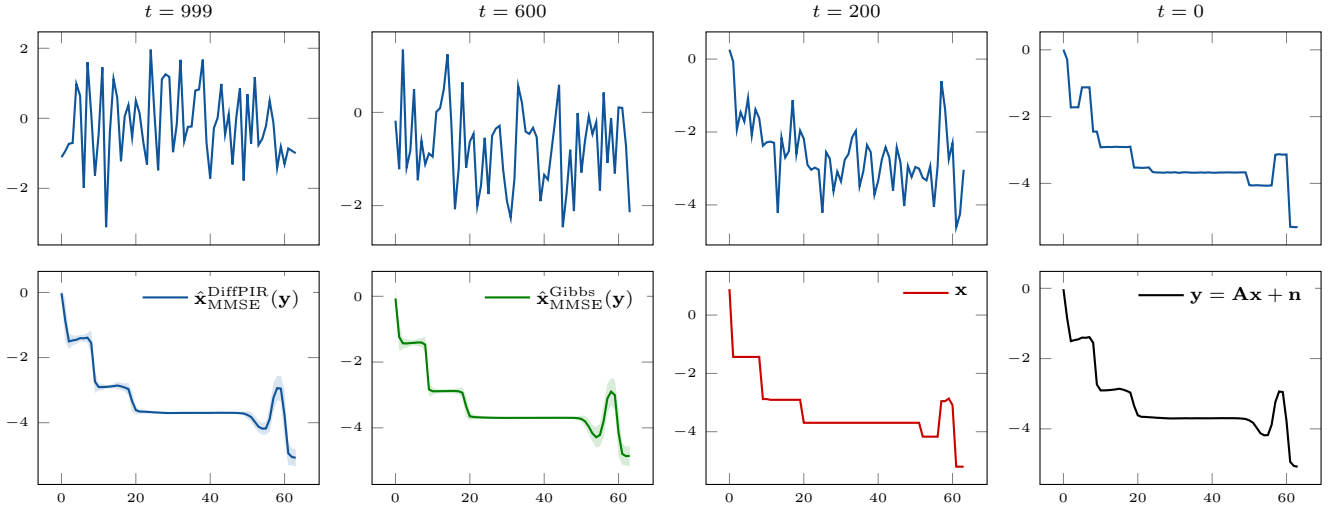


Fig. 9: Conditional generation for deconvolution of a signal with BL(0.1, 1) jumps with DiffPIR. Top: Prototypical sampling trajectory at times $t = 999, 600, 200, 0$. Bottom: From left to right: MMSE estimate obtained by averaging all DiffPIR samples; gold-standard MMSE estimate obtained by the Gibbs method; the data-generating signal; the data.

| Name | Distribution | Parameter(s) | Support | Notation |
|------------------------------|--|--|-----------------------|----------|
| Gaussian | $\frac{1}{\sqrt{2\pi}\sigma^2} \exp\left(-\frac{(x-\mu)^2}{\sigma^2}\right)$ | $\mu \in \mathbb{R}, \sigma^2 \in \mathbb{R}_{>0}$ | \mathbb{R} | Gauss |
| Exponential | $\lambda \exp(-\lambda x)$ | $\lambda \in \mathbb{R}_{>0}$ | $\mathbb{R}_{\geq 0}$ | Exp |
| Laplace | $\frac{1}{2b} \exp\left(-\frac{ x }{b}\right)$ | $b \in \mathbb{R}_{>0}$ | \mathbb{R} | Laplace |
| Student-t | $\frac{\Gamma(\frac{\nu+1}{2})}{\sqrt{\pi\nu}\Gamma(\frac{\nu}{2})} \left(1 + \frac{x^2}{\nu}\right)^{-\frac{\nu+1}{2}}$ | $\nu \in \mathbb{R}_{>0}$ | \mathbb{R} | St |
| Gamma | $\frac{\beta^\alpha}{\Gamma(\alpha)} x^{\alpha-1} \exp(-\beta x)$ | $\alpha, \beta \in \mathbb{R}_{>0}$ | $\mathbb{R}_{>0}$ | Gamma |
| Generalized inverse Gaussian | $\frac{(\frac{a}{b})^{\frac{p}{2}}}{2K_p(\sqrt{ab})} x^{p-1} \exp\left(-\frac{ax+b/x}{2}\right)$ | $a, b \in \mathbb{R}_{>0}, p \in \mathbb{R}$ | $\mathbb{R}_{>0}$ | GIG |
| Bernoulli-Laplace | $\lambda \delta(x) + (1-\lambda) \frac{1}{2b} \exp\left(-\frac{ x }{b}\right)$ | $\lambda \in [0, 1], b \in \mathbb{R}_{>0}$ | \mathbb{R} | BL |

Γ denotes the gamma function defined as $\Gamma(x) = \int_0^\infty t^{x-1} \exp(-t) dt$ for any $x \in \mathbb{R}_{>0}$.
 K_ν denotes the modified Bessel function of the second kind with parameter ν .

TABLE V: Summary of univariate distributions used throughout this work.

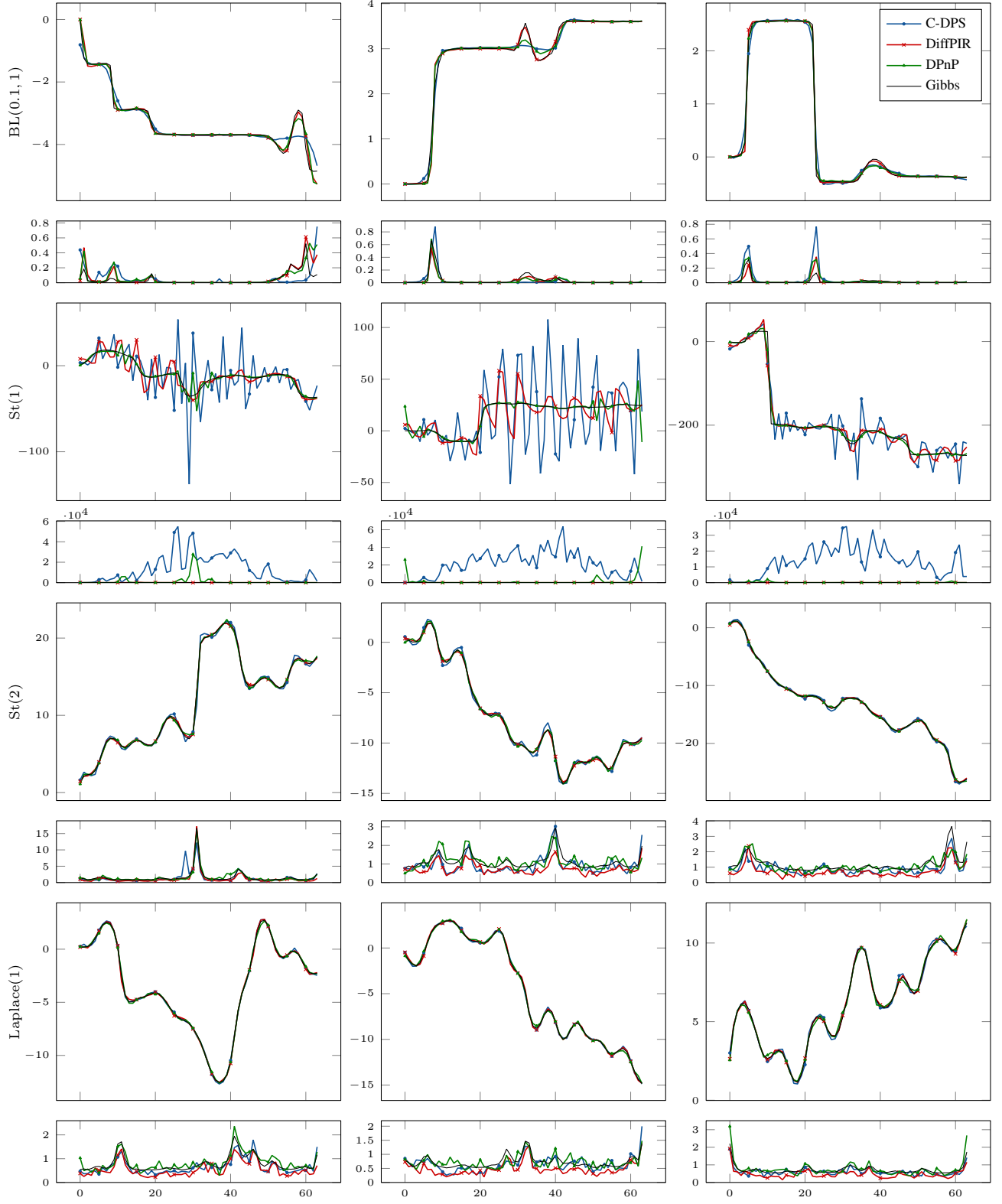


Fig. 10: Qualitative results for deconvolution using the learned denoiser. Rows: Jump distributions. For each jump distribution, the MMSE estimates obtained by the different DPS algorithms and the gold-standard Gibbs methods are shown on top of the corresponding index-wise marginal variances. Columns: Different measurements.

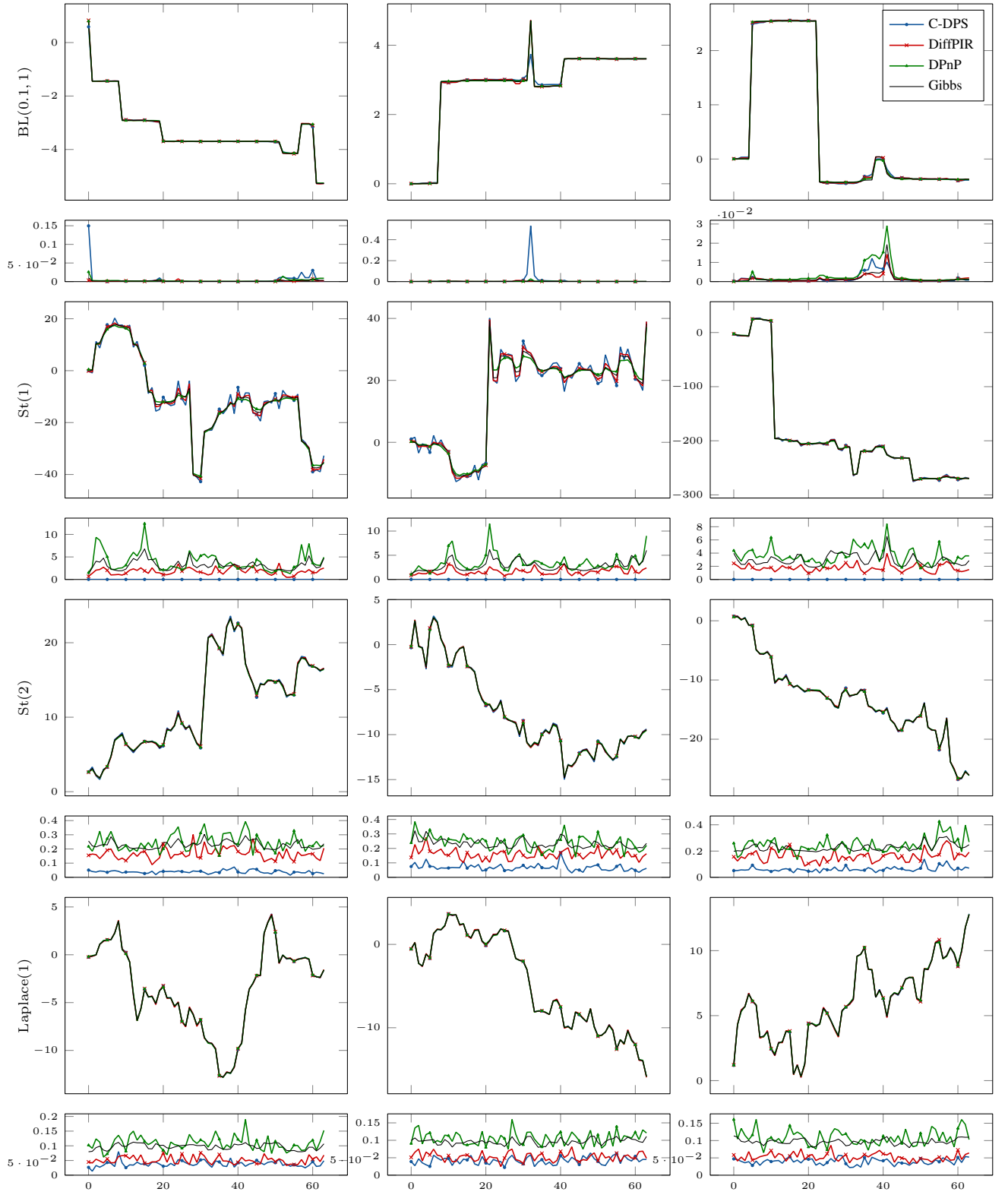


Fig. 11: Qualitative results for denoising using the oracle MMSE denoiser. Rows: Jump distributions. For each jump distribution, the MMSE estimates obtained by the different DPS algorithms and the gold-standard Gibbs methods are shown on top of the corresponding index-wise marginal variances. Columns: Different measurements.

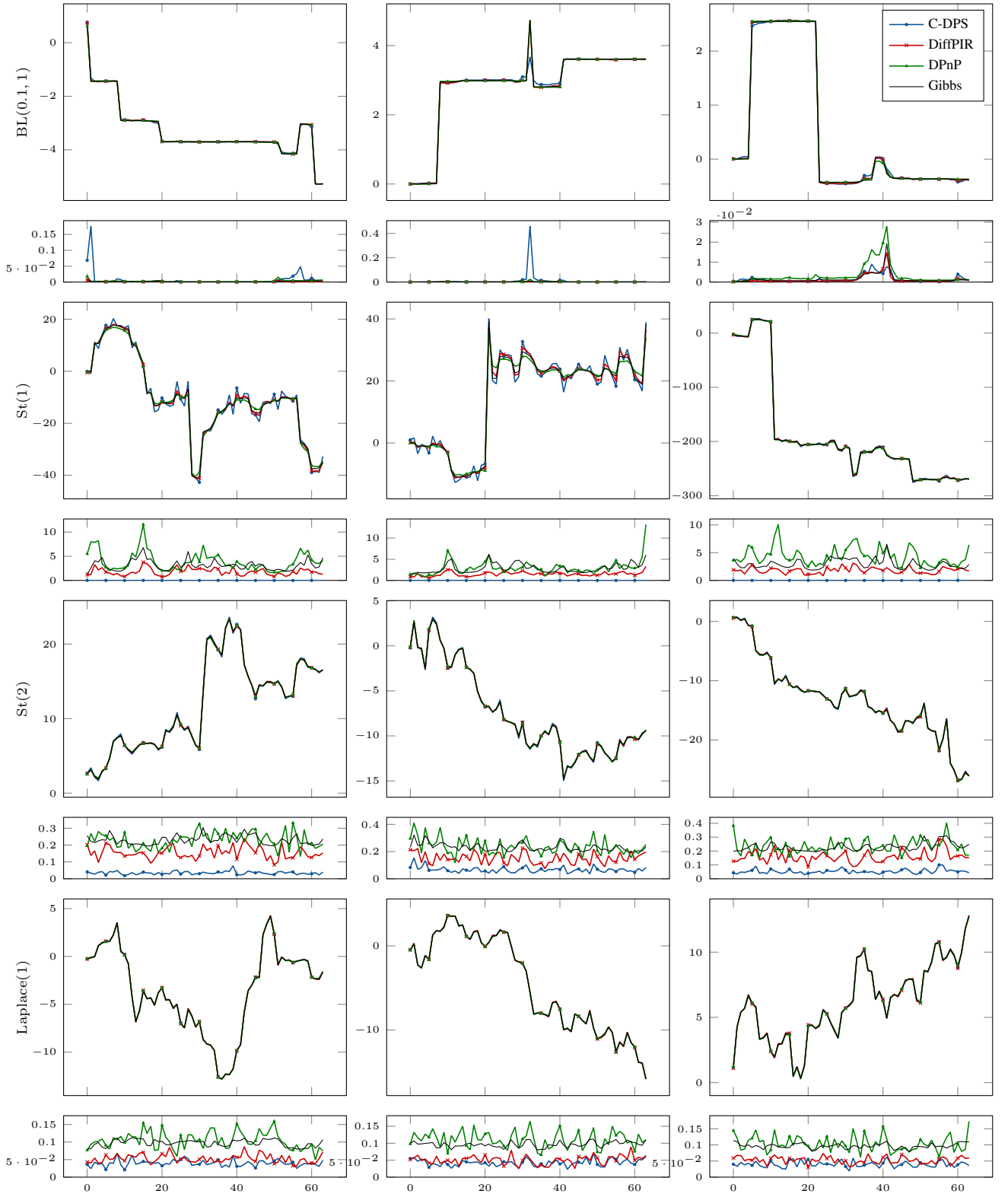


Fig. 12: Qualitative results for denoising using the learned denoiser. Rows: Jump distributions. For each jump distribution, the MMSE estimates obtained by the different DPS algorithms and the gold-standard Gibbs methods are shown on top of the corresponding index-wise marginal variances. Columns: Different measurements.

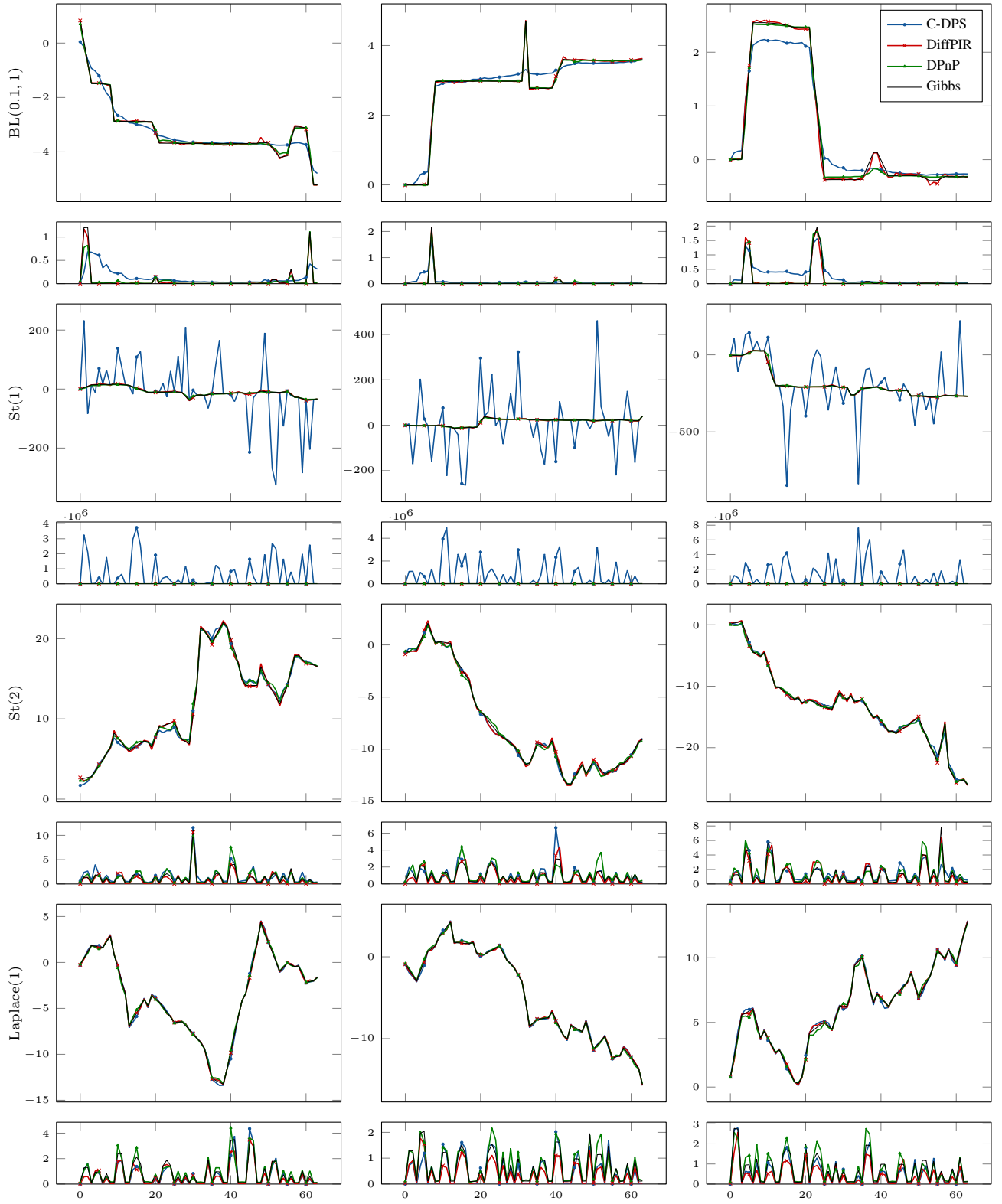


Fig. 13: Qualitative results for imputation using the oracle sampler. Rows: Jump distributions. For each jump distribution, the MMSE estimates obtained by the different DPS algorithms and the gold-standard Gibbs methods are shown on top of the corresponding index-wise marginal variances. Columns: Different measurements.

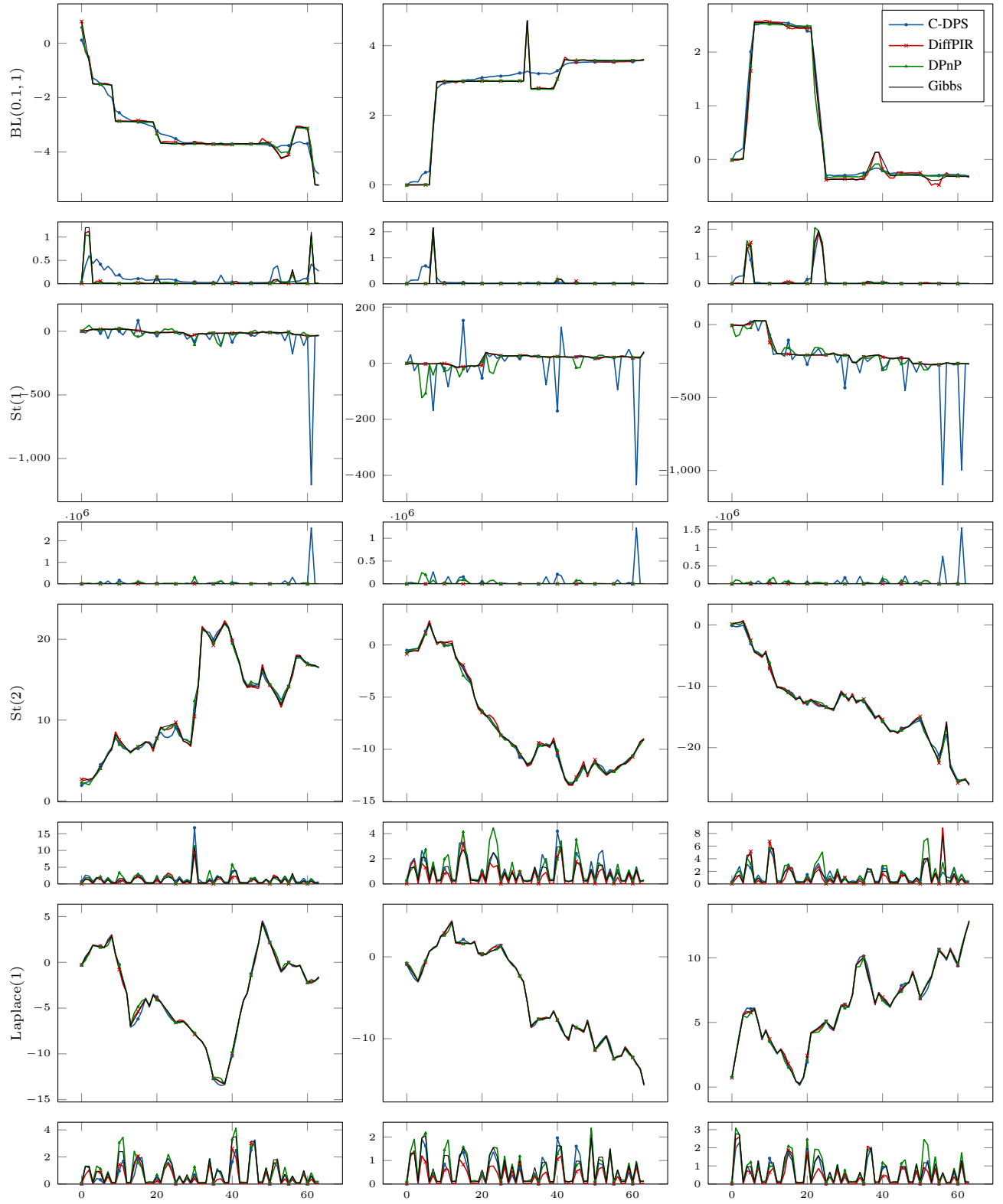


Fig. 14: Qualitative results for imputation using the learned denoiser. Rows: Jump distributions. For each jump distribution, the MMSE estimates obtained by the different DPS algorithms and the gold-standard Gibbs methods are shown on top of the corresponding index-wise marginal variances. Columns: Different measurements.

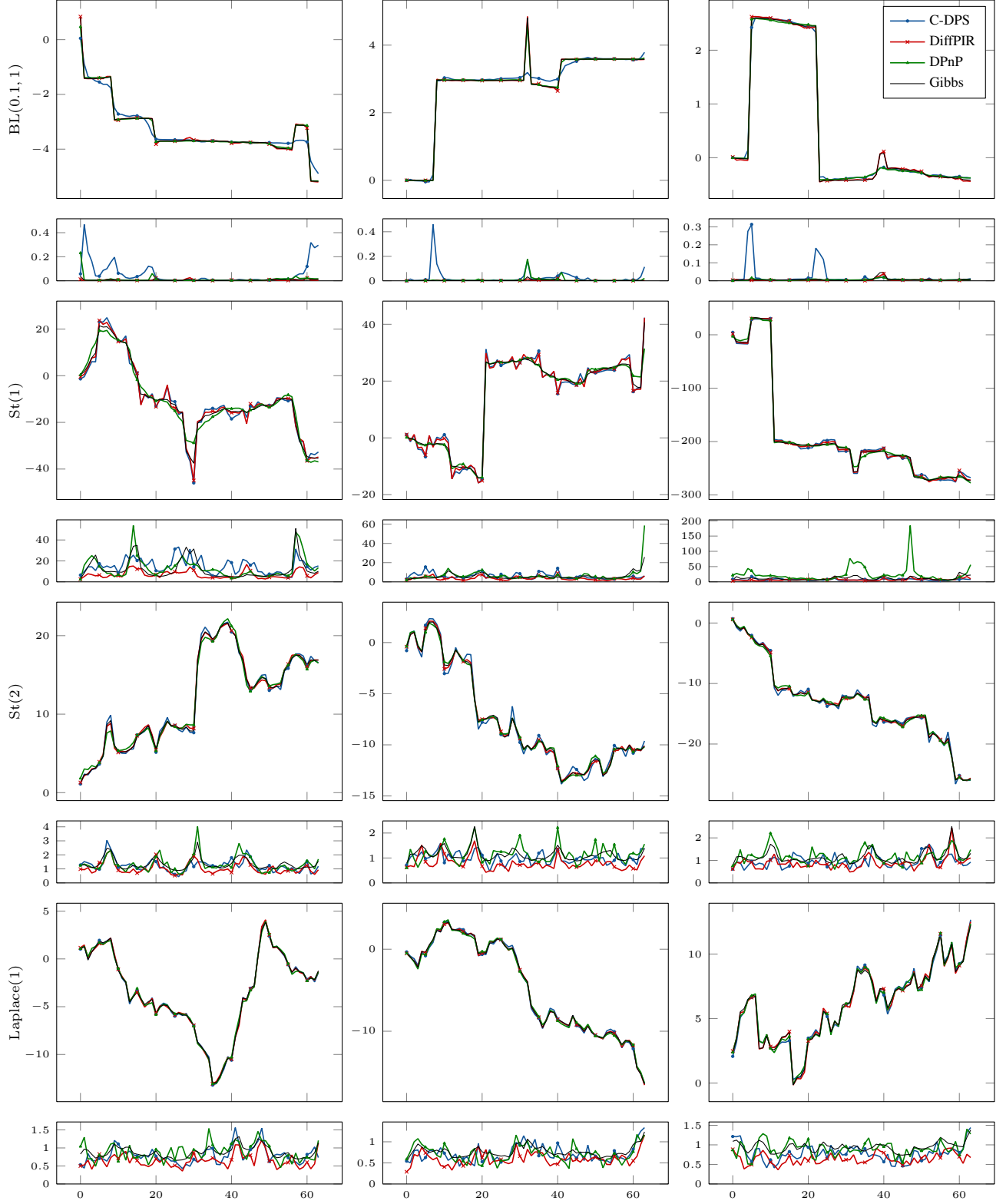


Fig. 15: Qualitative results for reconstruction from partial Fourier measurements using the oracle denoiser. Rows: Jump distributions. For each jump distribution, the MMSE estimates obtained by the different DPS algorithms and the gold-standard Gibbs methods are shown on top of the corresponding index-wise marginal variances. Columns: Different measurements.

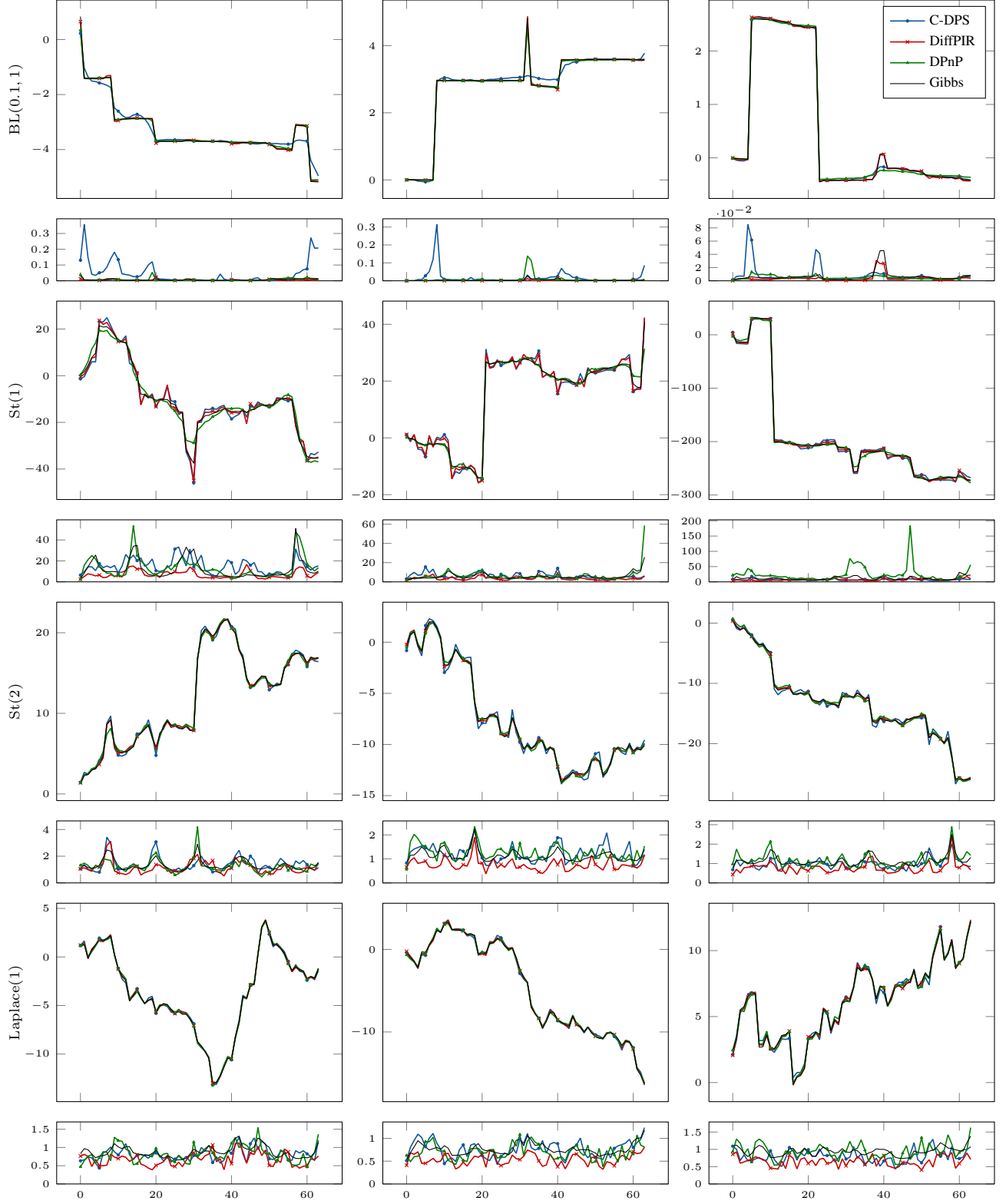


Fig. 16: Qualitative results for reconstruction from partial Fourier measurements using the learned denoiser. Rows: Jump distributions. For each jump distribution, the MMSE estimates obtained by the different DPS algorithms and the gold-standard Gibbs methods are shown on top of the corresponding index-wise marginal variances. Columns: Different measurements.

| Type | Distribution ϕ_i | Latent distribution f_i | Latent maps | Conditional latent distribution $p_{Z_i X=(\mathbf{K}\mathbf{x})_i}$ |
|-----------|--------------------------|---|---|--|
| Gauss | Gauss(μ, σ^2) | $\delta(0)$ | $\mu_i(z_i) = \mu, \sigma_i^2(z) = \sigma^2$ | $\delta(0)$ |
| Laplace | Laplace(b) | $\text{Exp}\left(\frac{1}{2b^2}\right)$ | $\mu_i(z_i) = 0, \sigma_i^2(z_i) = z_i$ | $\text{GIG}\left(\frac{1}{b^2}, (\mathbf{K}\mathbf{x})_i^2, \frac{1}{2}\right)$ |
| Student-t | St(ν) | $\text{Gamma}\left(\frac{\nu}{2}, \frac{\nu}{2}\right)$ | $\mu_i(z_i) = 0, \sigma_i^2(z_i) = \frac{1}{z_i}$ | $\text{Gamma}\left(\frac{\nu+1}{2}, \frac{\nu+(\mathbf{K}\mathbf{x})_i^2}{2}\right)$ |

TABLE VI: Latent variable representations and conditional distributions for common distributions.